

Description of rotating $N = Z$ nuclei in terms of isovector pairing.

A. V. Afanasjev^(1,2), S. Frauendorf^(1,3)

¹*Department of Physics, University of Notre Dame, Notre Dame, Indiana 46556, USA*

²*Laboratory of Radiation Physics, Institute of Solid State Physics, University of Latvia,
LV 2169 Salaspils, Miera str. 31, Latvia*

³*IKH, Research Center Rossendorf, Dresden, Germany*

(August 16, 2018)

Abstract

A systematic investigation of the rotating $N = Z$ even-even nuclei in the mass $A = 58 - 80$ region has been performed within the frameworks of the Cranked Relativistic Mean field, Cranked Relativistic Hartree Bogoliubov theories and cranked Nilsson-Strutinsky approach. Most of the experimental data is well accounted for in the calculations. The present study suggests that there is strong isovector np -pair field at low spin, the strength of which is defined by the isospin symmetry. At high spin, the isovector pair field is destroyed and the data are well described by the calculations assuming zero pairing. No clear evidence for the existence of the isoscalar $t = 0$ np -pairing has been obtained in the present investigation.

PACS: 21.60.Cs, 21.60Jz, 27.90.+b, 21.10.Pc

I. INTRODUCTION

It is well known that in the nuclei away from the $N = Z$ line proton-proton (pp) and neutron-neutron (nn) pairing dominate. In the $N \approx Z$ nuclei, protons and neutrons occupy the same levels. Strong np pair correlations are expected because of large spatial overlap of their wave functions. These correlations can be isoscalar and isovector. Figuring out their character and whether they form a static pair condensate (an average field) in respective channel has been a challenge since medium mass $N = Z$ nuclei have come into reach of experiment.

Shell model calculations show that there is strong isovector np -pairing the strength of which is fixed by isospin conservation [1,2] and that all three isovector components (nn, pp, np) are rapidly suppressed by increasing the angular momentum [3]. The isoscalar correlations are weaker and do not change much with angular momentum. These results can be interpreted by the presence of a static isovector pair field that is destroyed by rotation, like in nuclei far from the $N = Z$ line, and by the existence of dynamical isoscalar correlations that represent fluctuations around the zero mean value. The effective forces used in these calculations reproduce very well binding energies and other properties of $N \approx Z$ nuclei with $A < 60$, and thus should well estimate the relative strength of the isoscalar and isovector np pair correlations. On the other hand, one may not exclude that these comparisons are not sufficiently specific concerning np pair correlations. The analysis of pairing vibrations around ^{56}Ni indicates a collective behavior of the isovector pairing vibrations but do not support any appreciable collectivity in the isoscalar channel [4,5]. Refs. [6–8] demonstrated that the relative energies of the lowest $T = 0, 1/2, 1, 3/2$, and 2 states can be well accounted for by an isovector pair gap and a symmetry energy term proportional to $T(T + 1)$. Having these results in mind, a natural approach seems starting with the assumption that there is a strong isovector np pair field, the strength of which is determined by isospin conservation, and no isoscalar pair field. In this publication, we shall compare the rotational spectra of $N \approx Z$ nuclei with mean field calculations based on this assumption.

The strength of the isovector np -pairing is well defined by the isospin symmetry. A number of experimental observables such as binding energies of the $T = 0$ and $T = 1$ states in even-even and odd-odd $N = Z$ nuclei [8,7,9], the observation of only one even-spin $T = 0$ band in ^{74}Rb [9] instead of two nearly degenerate bands expected in the case of no $t = 1$ ¹ np -pairing clearly point on the existence of pairing condensate in this channel.

On the contrary, the strength of the isoscalar $t = 0$ np -pairing is not well known. Hence it is important to find physical properties that are sensitive to it and may provide evidence for its presence. In a number of publications it was suggested that the rotational properties of the $N \approx Z$ nuclei can serve for this purpose. However, in most of the cases these suggestions were based on the cranked shell model (CSM) ignoring the considerable softness of the shape of the nuclei in the mass region of interest.

In the present manuscript, the cranked Nilsson-Strutinsky (CNS) approach [10–12], the cranked Relativistic Mean Field (CRMF) [13–15] and the cranked Relativistic Hartree-

¹The lower-case letter t is used for the isospin of the pair-field in order to avoid the confusion with the total isospin of the states denoted by T .

Bogoliubov (CRHB) [22,16] theories (see Sect. II), which treat deformation properties more self-consistently than CSM, are employed for a detailed study of the rotating $N \approx Z$ nuclei in the mass range $A = 64 - 80$. Together with previously published results [17–19], they cover the mass range $A = 58 - 80$. These theories have successfully been tested in a systematic way on the properties of different types of rotational bands such as normal-deformed [20,21] and superdeformed [18,15,22,16] bands in the regimes of weak and strong pairing, as well as for smooth terminating bands [11,12,23]. Thus, their accuracy for the nuclei away from the $N = Z$ line is well established with respect of which the accuracy of the description of the $N \approx Z$ nuclei can be judged. Compared with other theories, such as total routhian surface (TRS) calculations [24], projected shell model (PSM) [25] and complex EXCITED VAMPIR approach [26], no adjustable parameters specific for nuclei in this mass region were used in our calculations.

Although these theories do not take implicitly into account the np -pairing, their use is justified by the study of the isovector mean field theory in Ref. [27]. The isovector pair field breaks the isospin symmetry. Therefore, many solutions of the Hartree-Bogoliubov (HB) equations exist, which correspond to different orientations of the pair field in isospace. One particular orientation corresponds to the case of no np pair-field. The np pair correlations are taken into account by restoring the isospin symmetry by means of approximate methods that correspond to the rotor or cranking models in the analogous case of breaking of the angular momentum symmetry in deformed nuclei.

The article is organized as follows. In Section II the main features of our theoretical tools are outlined. Necessary details of the calculations are also given. In Section III the accuracy of the employed methods is investigated for selected $N = Z + 2$ nuclei. The structure of even-even $N = Z$ with $64 \leq A \leq 80$ nuclei is investigated in Section IV. The question whether there is evidence for the existence of an isoscalar np -pair field is discussed in Section V. Section VI summarizes our main conclusions.

II. THEORETICAL TOOLS

The cranked Nilsson-Strutinsky approach [10–12], the cranked Relativistic Mean Field [13–15] and the cranked Relativistic Hartree-Bogoliubov [22,16] theories are employed in this manuscript for a detailed study of the rotating $N \approx Z$ nuclei. For high spin ($I \geq 15\hbar$) we neglect the pair correlations using the CRMF theory or the CNS approach. In the RMF approach the nucleus is described as a system of point-like nucleons represented by Dirac-spinors and coupled to mesons and to the photon. The nucleons interact by the exchange of several mesons, namely, the scalar σ and three vector particles ω , ρ and the photon. The CRMF theory represents the extension of RMF theory to the rotating frame. In the CNS approach the total energy is described as a sum of the rotating liquid drop energy and the shell correction energy. Although being much simpler than the self-consistent CRMF theory, the CNS approach provides a reasonable description of the nuclear many-body problem [12].

The CNS approach has several advantages compared to the self-consistent mean field models. These are the abilities (i) to specify a configuration in terms of occupation of low- and high- j orbitals, (ii) to trace fixed configuration up to the final termination in a non-collective state, (iii) to study the same configuration at given spin in different local minima (such as collective and non-collective or positive and negative γ -deformation). Implementing

them into the self-consistent theories requires the constraints on the configuration, spin and deformation over large deformation space. As a result, such calculations are not numerically feasible nowadays. Thus, in many cases the CRMF calculations (which are restricted to collective configurations only) are guided by the CNS results.

CRMF and CRHB+LN calculations have been performed with the NL3 parameterization of the RMF Lagrangian [28] which provides rather good description of nuclear properties throughout nuclear chart. The D1S Gogny force [29] and approximate particle number projection by means of the Lipkin-Nogami (LN) method have been used in the pairing channel of the CRHB+LN theory. The CRMF and CRHB+LN equations are solved in the basis of an anisotropic three-dimensional harmonic oscillator in Cartesian coordinates with the deformation parameters $\beta_0 = 0.3$, $\gamma = 0^\circ$ and oscillator frequency $\hbar\omega_0 = 41A^{-1/3}$ MeV. All fermionic and bosonic states belonging to the shells up to $N_F = 12$ and $N_B = 16$ are taken into account in the diagonalization of the Dirac equation and the matrix inversion of the Klein-Gordon equations, respectively. The detailed investigation indicates that this truncation scheme provides good numerical accuracy.

In order to investigate the dependence of the results on the parametrization of the Nilsson potential, the CNS calculations have been performed with the standard set of parameters [10] and the set suggested for the $A \sim 80$ mass region in Ref. [30] ('A80' parameter set in the following).

In the calculations without pairing, the shorthand notation $[p, n]$ indicating the number $p(n)$ of occupied $g_{9/2}$ proton (neutron) orbitals is used for labeling of the configurations. In the cases when the holes in the $f_{7/2}$ subshell play a role, an extended shorthand notation $[(p_h)p, (n_h)n]$ with $p_h(n_h)$ being the number of proton (neutron) $f_{7/2}$ holes is used. Since high- j $f_{7/2}$ holes are important mainly in nuclei around ^{60}Zn [18], in many cases we consider only mixed low- j $N = 3$ orbitals and use 3_i label for them, where subscript i indicates the position of the orbital within the specific signature group. An appreciable number of configurations should be considered when the calculations are performed as a function of ω in order to establish which configurations are lowest in energy at given spin and which ones have to be compared with experimental data.

III. ACCURACY OF THE MEAN-FIELD DESCRIPTION IN THE MASS 60-80 REGION

It is well known that the shape of the nuclei in the mass 60-80 region changes strongly both with angular momentum and with configuration. They are characterized by considerable softness of potential energy surfaces [31]. At high spin, superdeformation [17] and the termination of rotational bands [32,33] play an important role. These features must be taken into account when discussing the evidence for np pairing. As examples for the dramatic shape changes and band termination features encountered in this mass region we study $^{73,74}\text{Kr}$ and ^{70}Br nuclei in the framework of the CNS and CRMF theories. Since it is expected that proton-neutron pairing is not important in the $N = Z + 2$ nucleus ^{74}Kr [34], the results for this nucleus provide a benchmark for the accuracy of the description of rotational properties within the CRHB+LN theory.

A. Unpaired regime: ^{74}Kr .

Fig. 1 shows the excitation energies of several configurations, forming the yrast line of four combinations of parity and signature, obtained in the CNS calculations with the standard and 'A80' sets of the Nilsson parameters. Since the two sets differ in the energies of various single-particle orbitals, the relative energies of the configurations depend strongly on the parametrization. For example, the proton $f_{7/2}$ spherical subshell is located too high in energy in the 'A80' set. As a consequence, the signature degenerated [(1)3,4] configurations involving a hole in $\pi f_{7/2}$ compete with the [3,4] configurations (Fig. 1b). However, in experiment such bands have not been observed (see discussion below). The calculations with the standard Nilsson parameters place such bands more than 1 MeV above the yrast line (Fig. 1d), in much closer correspondence with the experimental situation. The [3,3] configurations, involving one neutron in the $3_4(\alpha = \pm 1/2)$ orbitals, are more energetically favored in the standard Nilsson set than in the 'A80' set, reflecting the different energy spacing between the $\nu g_{9/2}$ orbitals and the above mentioned orbitals in these sets. The experiment seems to favor the energy spacing between the orbitals obtained in the 'A80' set (see below).

The CNS calculations (Fig. 1) predict the existence of a number of aligned states and the states with small collectivity ($\gamma \sim 40^\circ$ and larger) along the yrast line. In addition, collective and non-collective minima coexist within the specific configurations (see Sect. 6.5 in Ref. [12] for a detailed discussion of such coexistence). The relative energies between these minima depend strongly on the Nilsson parametrization (for example, compare [2,2] configurations in Figs. 1a and c). At present, no aligned or weakly collective states of this kind have been observed in ^{74}Kr . Because of the predicted small collectivity of these states as well as of their irregular character, they are expected to be much more difficult to be observed than the more collective configurations. Although states of this kind competing with more regular collective bands have been predicted for a number of nuclei in the $A \sim 80$ mass region in different models [31,12], they have only been observed in ^{84}Zr so far [35].

The rotational properties of specific collective configurations, reflected in the $(E - E_{RLD})$ curves (see Figs. 1 and 2), the moments of inertia (Fig. 3) and the effective alignments i_{eff} (Fig. 4), are less sensitive to the parametrization of the Nilsson potential. Thus, we use these properties for assigning configurations to observed bands. These assignments rely not only on the results of the CNS calculations, but also on the results of the CRMF calculations, which give a very similar collective spectra. The minor differences are discussed below.

The configuration [2,4]($\alpha = 0$) is assigned to positive parity band 1, while [3,4]($\alpha = 0$) and [3,4]($\alpha = 1$) to the negative parity bands 3 and 2 (Fig. 2), respectively. The [3,4]($\alpha = 0, 1$) configurations are created from [2,4]($\alpha = 0$) by an excitation of the proton from the $3_3(\alpha = \pm 1/2)$ orbits into third $g_{9/2}$ orbit. The slopes, relative energies and the positions of the minima in the $(E - E_{RLD})$ plot (Fig. 2a,b), and, consequently, the dynamic and kinematic moments of inertia (Fig. 3a-c) of bands 1-3 are very well reproduced by these configurations. The calculated effective alignments of band 3 in ^{73}Kr (3) and bands 1, 2 and 3 in ^{74}Kr are close to experiment (Figs. 4d,e,f) at rotational frequency above 1 MeV where pairing is expected to be negligible.

These configurations are also the lowest collective configurations in the CRMF calculations. Concerning the excitation energies, the CRMF results are quite similar to the CNS ones shown in Fig. 2: the minima in the $(E - E_{RLD})$ curves are obtained at $I = 26\hbar$,

$I = 30\hbar$ and $I = 29\hbar$, respectively, in close agreement with experiment (see Fig. 2b). Also the relative energies, the slopes of the $(E - E_{RLD})$ curves of bands 1-3 and the spins at which bands 2 and 3 cross band 1 are well reproduced by the CRMF calculations. At $\omega \geq 1.0$ MeV, the kinematic moments of inertia of these bands are well reproduced, while dynamic moments of inertia are somewhat underestimated (Fig. 3a-c). The rise in $J^{(2)}$ in the configuration assigned to band 3 at $\omega \sim 1.65$ MeV (Fig. 3c) is due to the crossing of the $\nu g_{9/2}(\alpha = -1/2)$ and $\nu(g_{7/2}d_{5/2})(\alpha = -1/2)$ orbitals. The effective alignments of the band pairs $^{73}\text{Kr}(3)-^{74}\text{Kr}(1,2,3)$ are close to experiment (Figs. 4d,e,f).

Comparing experimental and calculated $(E - E_{RLD})$ curves (Fig. 2) and effective alignments i_{eff} (Fig. 4h), we assign the unpaired configuration $[4, 4](\alpha = 0)$ to band 5 at high spin (above $I = 16\hbar$). While the energy differences between band 5 and bands 2 and 3 are well reproduced in both parametrizations, only the standard Nilsson parameters reproduce the excitation energy of band 5 with respect of band 1. Considering the differences in the configurations of these bands (see Fig. 4), one can conclude that the energy gap between the $\pi 3_3(\alpha = \pm 1/2)$ and $\pi g_{9/2}$ orbitals is much better described with the standard Nilsson parameters than with the 'A80' ones. This is clearly seen in the relative energies of bands 1, 2 and 3 in ^{74}Kr (Fig. 2) and bands 1, 2 and 3 in ^{73}Kr (see Fig. 6 in Ref. [38] for the results with the 'A80' set), which are sensitive to the energy gap between the above mentioned orbitals. These relative energies are better reproduced by the standard Nilsson parameters.

Our configuration assignment of band 5 agrees with that obtained within the TRS framework [40], where it was suggested that the lowest 2qp positive-parity band (band 5) is built on the $(\pi g_{9/2})^2$ (AB) configuration which undergoes band crossing at $\omega \sim 0.9$ MeV due to the alignment of the $(\nu g_{9/2})^2$ neutron pair.

The interpretation of band 6 is more ambiguous, because it is not linked to the low-spin level scheme. Using the effective alignment, we suggest that it is based on the $[3, 3](\alpha = 0)$ configuration (see Fig. 4i) and its lowest state has spin $I_0 = 8\hbar$. Assuming this spin, the slope of experimental $(E - E_{RLD})$ curve is well reproduced (Fig. 2). The weak point of this interpretation is the fact that the $[3, 3](\alpha = 1)$ configuration is predicted to have a lower energy (especially in the 'A80' set) than this configuration (Fig. 1a and c). However, both in the CNS calculations with the standard parameters and in the CRMF calculations it is lower in energy by only few hundred keV in the short spin range $I = 23 - 27\hbar$. This difference in predicting the relative energies of the lowest $[3, 3](\alpha = 0, 1)$ configurations can be traced to the signature splitting of the $\nu 3_4(\alpha = \pm 1/2)$ orbitals.

The fact that the $[3, 3](\alpha = \pm 1/2)$ configurations have been observed in ^{73}Kr (bands 1 and 2) [38], strongly suggests the presence of similar configurations in ^{74}Kr . Indeed, by adding one $3_4(\alpha = \pm 1/2)$ neutron to these configurations of ^{74}Kr , four $[3, 3]$ configurations are created (Fig. 1a and c). In the CRMF calculations, these $[3, 3]$ configurations are somewhat less energetically favored with respect of the $[2, 4]$ configuration used as a reference in comparison with the CNS calculations.

Since band 4 does not reach the region of weak pairing (Fig. 3d), an unambiguous interpretation of this band in the formalism without pairing is difficult. However, since the signature partner of this band has not been observed, the signature degenerated $[(1)3, 4]$ configurations can be excluded. Thus, only decoupled $[2, 3](\alpha = 1)$ configuration (Fig. 1b and d) seems to be a reasonable candidate for the extension of this band to high spin. The analysis of the CRMF results leads to the same conclusion.

B. Unpaired regime: ^{73}Kr

This nucleus has been studied in detail in Ref. [38] by means of the CRMF theory and the CNS approach employing the 'A80' Nilsson parameters. In addition, we have carried out a CNS study with the standard parameters for the Nilsson potential, which gave similar results, where, however, the relative energy of band 3 and bands 1 and 2 is better reproduced (see Sect. III A). At $\omega \geq 1.0$ MeV, the calculations without pairing (CNS and CRMF) reproduce well experimental data; see Figs. 6 and 7 in Ref. [38].

C. Softness of the $N \sim Z$ nuclei: ^{70}Br

Selected potential energy surfaces of ^{70}Br in Fig. 5 illustrate the soft nature of the $N = Z$ nuclei in the $A \sim 70$ mass region. They also show that the height of the barrier between the minima at $(\varepsilon_2 \approx 0.35, \gamma \sim -20^\circ)$ and $(\varepsilon_2 \approx 0.35, \gamma \sim 30^\circ)$ depends on the parametrization of the Nilsson potential. On the other hand, the relative energies of these two minima and their deformations are less sensitive to the parametrization of the Nilsson potential.

In the $N = Z$ nuclei with particle numbers 34, 35, and 36 the observed bands are associated with either the [2,2] or [3,3] configurations, residing in these two competing local minima, or both of them. The high spin part of the band HB1 in ^{70}Br is the envelope of the [3,3] configurations [50]. The CNS calculations also indicate the existence of collective [2,2] configurations associated with similar two local minima (see Ref. [50] for details and Fig. 6), but they have not been observed in experiment. The [2,2] configurations dominate the yrast line in ^{68}Se because of the lower Fermi level. The bands belonging to such a structure have been observed (see Sect. IV B). The bands with [2,2] and [3,3] configurations have been observed in ^{72}Kr (see Sect. IV C).

D. CRHB+LN theory: ^{74}Kr

Fig. 7b compares the kinematic moment of inertia of ^{74}Kr calculated within the CRHB+LN theory with the experimental data. With exception of the lowest frequency point and two points after band crossing the experimental data is excellently reproduced by the configuration that is lowest in energy in the near-prolate minimum. The lowest frequency point is well reproduced by the oblate configuration, which suggests a transition from oblate to prolate shape at $I \sim 4\hbar$ within the ground state band of ^{74}Kr . The band crossing is caused by the simultaneous alignment of the proton and neutron $g_{9/2}$ pairs. No convergence has been obtained for $\omega \geq 1.21$ MeV due to very weak pairing at these frequencies. However, the similarity of the CRHB+LN and CRMF results for $J^{(1)}$ above the band crossing suggests that the weak $t = 1$ pairing only insignificantly modifies the rotational properties. The same result has been obtained in ^{72}Kr (Fig. 7a) and in ^{60}Zn (Ref. [42]). The CRHB+LN calculations reproduce well the transition quadrupole moment Q_t of the ground state band and its dramatic drop after the band crossing (see Fig. 8). These calculations together with the CRMF calculations for the [2,4] configuration (unpaired analog of the S-band) indicate a gradual decrease of Q_t with increasing spin. It is caused by a decrease of β_2 and an increase of γ -deformation.

E. ^{78}Sr

A delay of the first band crossing in the ground state band of even-even $N = Z$ nucleus with respect to the one in the $N = Z + 2$ nucleus has been widely discussed as an evidence for the $t = 0$ np -pairing [43]. However, in order to apply this argumentation the band crossing frequency has to be well established in the $N = Z + 2$ system. While this is unproblematic in ^{74}Kr (see Sect. III D), the situation in ^{78}Sr is more complicated. The detailed discussion below illustrates this.

To facilitate the discussion of positive parity bands of ^{78}Sr (see Fig. 3 in Ref. [40]) we use the label A for the branch consisting of the ground state band up to $I = 12^+$ state, and the states at the energies 6025 (14^+), 7559 (16^+), 9254 (18^+), 11195 (20^+) and 13294 (22^+) keV. The label B is used for the branch consisting of the states at the energies 9254 (18^+), 10995 (20^+), 12981 (22^+), 15233 (24^+) and 17764 (26^+) keV.

The results of the CRHB+LN and CNS calculations and experimental data are shown in Fig. 9. The branch B shows all features typical for the rotation in the unpaired regime such as $J^{(2)} \leq J^{(1)}$ and the smooth decrease of both quantities with increasing rotational frequency (Fig. 9b). This smoothness strongly suggests that the branch B is not affected by the interaction with another band. Note that the state at 9254 (18^+) keV is included in both branches. The smoothness of $J^{(2)}$ and $J^{(1)}$ with this state included in branch B (see Fig. 9b) suggests that this state belongs to band B not to band A. It is likely that the branch B is the continuation of the g-band above the point of crossing with the S-band at $I \sim 16\hbar$ (see below) and corresponds to the unpaired [4,6] configuration (compare panels (c) and (d) of Fig. 9). However, neither CRMF nor CNS calculations describe well the kinematic moment of inertia of branch B (Fig. 9b) under this configuration assignment. Similar problems with the description of this branch has been encountered also in the TRS calculations of Ref. [40].

The dip in $J^{(2)}$ of branch A at $\omega \sim 0.9$ MeV (Fig. 9a), which is not typical for paired band crossing, suggests that at this frequency the g-band is crossed by some other configuration. This means that the states at 11195 keV (20^+) and at 13294 keV (22^+) of the branch A do not belong to the g-band. We were not able to make configuration assignment for these two states.

The presence of two closely lying 14^+ states does not allow a certain assignment of one of them to the g-band although the intensities within the bands suggest that the state at 6025 MeV belongs to g-band. Thus we can only be more or less certain that the states up to 16^+ in branch A belong to the g-band. In this range, the CRHB+LN calculations reproduce well the experimental ($E - E_{RLD}$) plot (Fig. 9c) and the moments of inertia (Fig. 9a; see also discussion below).

Extrapolating the calculated CRHB+LN ($E - E_{RLD}$) curve of the g-band to the crossing point with the S-band predicts a back-bend at $I \sim 16\hbar$ (Fig. 9a). The calculated equilibrium deformation of S-band ($Q_t \sim 2.37$ eb, $\beta_2 \sim 0.28$ and $\gamma \sim -20^\circ$) differs considerably from the one of the g-band ($Q_t \sim 3.6$ eb, $\beta_2 \sim 0.47$ and $\gamma \sim -1^\circ$). After simultaneous alignment of the proton and neutron $g_{9/2}$ pairs, the pairing is weak in the S-band, and thus this band can be associated with the unpaired [4,4] configuration. A similar situation is found also in the CNS calculations where the [4,6] configuration (unpaired analog of the g-band) is crossed by the [4,4] configuration (unpaired analog of the S-band) at $I = 14\hbar$ (Fig. 9d). The deformations of these configurations are similar to those obtained in the CRHB+LN

calculations for the g- and S-bands. In addition, the CNS calculations indicate that the yrast line above $I = 14\hbar$ is formed by the weakly collective or non-collective aligned states. A configuration similar to the S-band of the CRHB+LN calculations has also been obtained in the TRS calculations of Ref. [40].

The CNS calculations suggest that one of two closely lying $I = 14^+$ states is either the aligned state of the [2,2] configuration (Fig. 9d) or the state of the [4,4] configuration (S-band) (Fig. 9c and d). The interaction between these two states might explain the discrepancy between the calculated and experimental $J^{(2)}$ values for g-band at $\omega \sim 0.7$ MeV (Fig. 9a).

The present results strongly suggest that the S-band has not been observed in ^{78}Sr , and, thus the use of this nucleus as a reference point in comparing band crossing frequencies is not justified. The situation is reminiscent to ^{72}Kr in the past, where the S-band was missing in the early experiments (see Sect. IV C). Additional experimental studies at $I \geq 14\hbar$ are needed in order to better understand the structure of ^{78}Sr .

The conclusion about non-observation of the S-band in ^{78}Sr is strongly supported by the analysis of both the complicated level scheme in neighboring ^{77}Rb nucleus, which has one proton less and the g- and S-bands in ^{76}Kr which has two proton less (see Fig. 7). In ^{77}Rb , the high spin bands P3 [44,45] and N2 [45] are associated with the [3,4] and [3,5] configurations, respectively, and their properties are well described by the CNS calculations [47]. For example, the crossing of two ($\pi = +, \alpha = +1/2$) bands P3 and P1 seen at $I = 18\hbar$ in experiment is well described by the crossing of the [3,6] and [3,4] bands. However, pairing is still playing a role in the band P1 so its low spin properties are not completely reproduced in the calculations without pairing. It is clear that one additional proton in the $g_{9/2}$ orbital, leading to the [4,6] and [4,4] configurations in ^{78}Sr discussed above, should not modify considerably the situation as have been seen in the Kr isotope chain (see Sects. III A, III B, IV C).

Our analysis reveals the problems in interpreting this $N = Z + 2$ nucleus by means of our theoretical methods. At present, it is not clear to which extend they are due to the deficiencies of the models or to incomplete data. However, this study clearly indicates that one has to be very careful to relate possible problems in understanding the experimental data on $N = Z$ nuclei to the lack of $t = 0$ np -pairing in the models.

F. Band termination

Above the rotational frequency of paired band crossings at $\omega = 0.6 - 1.0$ MeV, almost all experimental bands studied in this paper show the same feature: a drop of the dynamic moment of inertia below the kinematic one and decreasing kinematic moment of inertia with increasing rotational frequency. Such a behaviour is typical for smooth band termination [12], which is caused by limited angular momentum content of underlying single-particle configurations. Band termination corresponds to a gradual change from collective (near-prolate, triaxial) shape towards non-collective oblate shape, as illustrated in Fig. 10. As documented in Ref. [12], the CNS approach describes reliably such bands in nuclei away from the $N = Z$ line. As shown in the present manuscript the CNS and CRMF approaches describe the high-spin bands in the $N \approx Z$ nuclei with a comparable level of accuracy.

G. Single-particle spectra

The uncertainties in the energies of the single-particle states will affect the shell effects, which determine the positions of local minima in deformation plane and the barriers between these minima (see Sect. III C). The rotational properties and relative energies of configurations and their mutual interaction will also be affected. These properties will be less sensitive to inaccuracies of the single particle spectrum if the gap between interacting states is large. For example, the effective alignments of bands in $^{72,73,74}\text{Kr}$ which differ by the occupation of the $\pi 3_3(\alpha = \pm 1/2)$ orbitals are more sensitive to the parametrization of the Nilsson potential than those between the bands differing in the occupation of the $\pi g_{9/2}$ subshell (Fig. 4), because the relative energies of $\pi 3_2(\alpha = \pm 1/2)$ and $\pi 3_3(\alpha = \pm 1/2)$ orbitals and their interaction depend strongly on the parametrization.

H. Concluding remarks

The study of selected $N = Z + 2$ nuclei presented in this Section reveals a number of features typical for $N \approx Z$ nuclei with $60 < A \leq 80$. It illustrates the typical accuracy of the theoretical tools employed. The potential energy surfaces of these nuclei are shallow and shape coexistence is a common feature. The rotational bands show all the features of terminating bands at high spin. The process of band termination is associated with a drastic shape change from near-prolate (triaxial) shape at low spin towards non-collective oblate shape at high spin. The transition from the g-band to S-band is associated with a shape change as well. These phenomena cannot be ignored in studying the consequences of np -pairing for the properties of rotating nuclei. Our analysis also demonstrates that the results of the calculations depend on how accurately the energies of the single-particle states are reproduced. Hence, certain discrepancies between calculations and experiment seen in the $N = Z$ nuclei (Sect. IV) should not necessarily be attributed to the neglect of $t = 0$ np -pairing.

IV. THE STRUCTURE OF EVEN-EVEN $N = Z$ NUCLEI

The application of the isovector mean-field theory [27] to even-even $N = Z$ nuclei is very simple. Since all low-lying rotational bands have isospin $T = 0$, the calculations by means of the CRHB+LN model can be directly applied to rotational bands in these nuclei, because the isorotational energy term $T(T + 1)/2\mathcal{J}_{iso}$ vanishes. On the level of accuracy of the standard mean-field calculations, the restoration of the isospin symmetry (which takes care of the $t=1$ np pair field) changes only the energy of the $T = 1$ states relative to the $T = 0$ states [27]. The high spin states are systematically studied by means of the CSN and CRMF approaches, which assume zero pairing. Calculation of the low and intermediate spin states by means of the CRHB+LN theory for selected nuclei complement the study.

A. ^{64}Ge

It has been pointed out before that this nucleus is soft with respect to γ - and octupole deformations (see Ref. [48] and references quoted therein). Fig. 11 shows the results of the CNS calculations (restricted to reflection symmetric shapes), which also indicate softness toward γ -deformation. The $[0,0](\alpha = 0)$ configuration is characterized by the ($\varepsilon_2 \sim 0.2, \gamma \sim -30^\circ$) deformation in the spin range $I = 2 - 8\hbar$. The yrast lines of other combinations of parity and signature are characterized by similar deformation in the spin range $I = 0 - 3\hbar$. Up to spins $I \sim 35\hbar$, the yrast lines are dominated by the states with the deformations $\varepsilon_2 \approx 0.25 - 0.35$ and $\gamma = 26^\circ - 60^\circ$. Band terminations, mostly in a favored way [12], are typical for the yrast region up to $I \sim 35\hbar$. Superdeformed bands with deformation $\varepsilon_2 \sim 0.5, \gamma \sim 10^\circ$ become yrast above that spin.

It seems to us that the complicated structure of this nucleus, dominated in the spin region of interest by γ - (and probably octupole) softness and terminating structures, will not allow to obtain reliable evidences of the isoscalar $t = 0$ np -pairing even if the experimental data will be extended to higher spin.

B. ^{68}Se nucleus

As shown in Fig. 12a, the structure of ^{68}Se calculated by means of the CNS approach is quite complicated with different configurations competing for yrast status. However, the positive parity $[2, 2](\alpha = 0)$ configuration (shown by solid line with large solid circles) stays close to yrast line over a considerable spin range. Also the CRMF calculations indicate that this configuration is energetically favoured in the spin range of interest. However, it is yrast in the $(\pi = +, \alpha = 0)$ group of states only within some spin range. For example, the configurations $[1, 1](\alpha = 0)$ and $[21, 2](\alpha = 0)$ compete with it for yrast status at spins $I = 10 - 14\hbar$ and $I = 28\hbar$, respectively.

Fig. 12b compares the $[2, 2](\alpha = 0)$ configuration with the rotational sequences A and B observed in this nucleus [49]. For $I > 14\hbar$, the calculations are in almost perfect agreement with band A. The state at $I = 16\hbar$ has a deformation of $\varepsilon_2 = 0.326$ and $\gamma = 33^\circ$. With increasing spin the quadrupole deformation generally decreases but γ -deformation increases towards $\gamma = 60^\circ$ (Fig. 10). This is due to the limited angular momentum content of the configuration which leads to band termination [11,12]. The CNS calculations give two aligned states within this configuration. The state at $I = 28\hbar$, which corresponds to maximum spin, has the structure $\pi(g_{9/2})_8^2(f_{5/2}p_{3/2})_6^4 \otimes \nu(g_{9/2})_8^2(f_{5/2}p_{3/2})_6^4$. The state at $I = 24\hbar$ has the structure $\pi(g_{9/2})_8^2(f_{5/2}p_{3/2})_4^4 \otimes \nu(g_{9/2})_8^2(f_{5/2}p_{3/2})_4^4$ with a different alignment of the low- j $N = 3$ protons and neutrons (see Sect. 6.5 of Ref. [12] for a discussion of a similar situation in ^{158}Er). At $I = 24\hbar$, the potential energy surface indicates the coexistence of the non-collective aligned and more collective highly triaxial states within the $[2, 2](\alpha = 0)$ configuration.

For $\omega \approx 0.7 - 1.3$ MeV, the dynamic moment of inertia of band A is essentially flat (Fig. 13d) and it is significantly lower than the kinematic moment of inertia which decreases with increasing rotational frequency (Fig. 13a). This is a feature typical for rotational bands in unpaired regime approaching the limit of angular momentum that can be generated by the valence particles and holes (such as smooth terminating bands [11,12] and highly- and

superdeformed bands in the $A \sim 60$ mass region [18]). At $\omega \sim 1.4$ MeV, there is a rise in $J^{(2)}$. The CRMF calculations show that this is due to the crossing of two low- j $r = +i$ $N = 3$ single-particle orbitals both in proton and neutron subsystems. The CNS approach gives the same explanation for the rise of $J^{(2)}$.

The calculations indicate the coexistence of collective highly triaxial and noncollective aligned states at spin $I = 24^+$ within the $[2, 2](\alpha = 0)$ configuration. The analysis suggests that the observed $I = 24^+$ state in band A is the triaxial collective state shown by dashed line in Fig. 12b. It is reasonable to expect that the intensity of the $26^+ \rightarrow 24^+$ and $24^+ \rightarrow 22^+$ transitions will be much weaker if the 24^+ state is aligned as compared with the case when this state is collective. This is one possible reason why aligned $I = 24^+$ state has not been observed. It may also be that in reality this aligned state is less favoured in energy than predicted by the CNS. The terminating state at $I = 28^+$ has not been observed either. In the CNS calculations this state lies 0.8 MeV above the yrast line which suggests that it may not be well populated in experiment. The CRMF calculations also indicate the termination of the $[2, 2](\alpha = 0)$ configuration at $I = 28\hbar$ in the non-collective $\gamma = 60^\circ$ state, which is seen in Fig. 13b as the fact that the increase of ω above 1.6 MeV does not change I .

The CNS calculations suggest that the top part of the band B ($8 < I < 14\hbar$) corresponds to the collective ($\epsilon_2 \sim 0.33, \gamma \sim -35^\circ$) $[2, 2](\alpha = 0)$ configuration (Fig. 12b). The slope of the experimental ($E - E_{RLD}$) curve in this spin range is reasonably well reproduced, although the excitation energy is somewhat overestimated. The reason for the last discrepancy could be twofold: neglect of pairing correlations and the accuracy of the description of the energy difference between the minima with $(\epsilon_2 \sim 0.33, \gamma \sim 33^\circ)$ and $(\epsilon_2 \sim 0.33, \gamma \sim -35^\circ)$. The inclusion of pairing will decrease the excitation energy of the $(\epsilon_2 \sim 0.33, \gamma \sim -35^\circ)$ branch of the $[2, 2](\alpha = 0)$ configuration and will bend the $(E - E_{RLD})$ curve toward the experimental one. In addition, it will decrease the kinematic moment of inertia and aligned angular momentum towards the values seen in experiment (Fig. 13a and b). Despite the neglect of pairing the transition from negative- γ collective branch to the terminating branch at $I \sim 14\hbar$ (Fig. 12b) as well as the general features of kinematic moment of inertia (Fig. 13a) and aligned angular momentum (Fig. 13b) are well reproduced in the CNS calculations in the frequency range above 0.5 MeV.

In general, band B for $I > 8\hbar$ and band A have a structure very similar to the high-spin band (HB1) in ^{70}Br . In Ref. [50], this band was interpreted as built from two $[3, 3]$ configurations. The low- and medium- spin part of band was assigned to the $(\epsilon_2 \sim 0.35, \gamma \sim -20^\circ)$ local minimum, while top part of band to the $(\epsilon_2 \sim 0.35, \gamma \sim 30^\circ)$ minimum. Thus band B/A in ^{68}Se and HB1 band in ^{70}Br differ merely by one $g_{9/2}$ proton and one $g_{9/2}$ neutron, but they are located in the same local minima of potential energy surface. Similar $[2, 2]$ configurations as in ^{68}Se have also been predicted for ^{70}Br but have not been observed so far (see Ref. [50] for details).

In order to understand the low-spin structure, CRHB+LN calculations have been performed. At $I = 0\hbar$, the oblate minimum is lower than the prolate one by 0.8 MeV in very close agreement with experiment [51]. If the pairing is neglected the energy difference between two minima is smaller, because the pairing energy is larger in oblate minimum (1.67 MeV) than in prolate one (1.28 MeV). The CRMF calculations give a highly-deformed triaxial $[2, 2]$ configuration with $(\beta_2 \sim 0.42, \gamma \sim -20^\circ)$ which corresponds to the one in the CNS approach. At $I = 0\hbar$, it has an excitation energy of 3.2 MeV with respect of the

lowest state in the oblate minimum. At $I \sim 14\hbar$, it is crossed by the terminating branch of the [2,2] configuration. A comparison of the CRMF and CRHB+LN results for the prolate and oblate minima indicates that pairing has small effect on the equilibrium deformation. Assuming that this is also true for the highly-deformed triaxial minimum and that the gain in binding due to pairing is similar to the one in prolate and oblate minima, the above mentioned excitation energy is not far from the energy of band B extrapolated to spin $I = 0\hbar$, which is somewhat larger than 2 MeV.

The kinematic moments of inertia and aligned angular momentum of band C and the bottom branch of band B (spins $I = 2 - 6\hbar$) are compared with the CRHB+LN results in Fig. 13a,b and c. The calculations describe the experiment reasonably well, although some discrepancies are seen at $\omega \leq 0.55$ MeV. Due to convergency problems caused by weak pairing, the CRHB+LN calculations do not extend beyond 1.0 MeV. It is clearly seen that the CRHB+LN and CRMF results converge for $\omega \geq 0.8$ MeV (Fig. 13a). Both the prolate CRHB+LN solution ($\beta_2 \sim 0.24, \gamma \sim -3^\circ$) and the oblate one ($\beta_2 \sim 0.26, \gamma \sim -60^\circ$) are crossed by a band that contains an aligned $g_{9/2}$ proton pair and an aligned $g_{9/2}$ neutron pair ($\beta_2 \sim 0.34, \gamma \sim 25^\circ$), which corresponds to the unpaired [2,2]($\alpha = 0$) configuration.

The structure of this nucleus has been studied before. Apart from minor details, the TRS interpretation of bands C, B and of the bottom of band A [24] is in agreement with the one given above. However, the termination of band A has not been investigated. Projected shell model calculations for the oblate and prolate minima were performed in Ref. [52]. The interpretation of band C and bottom part of band B (spins $I = 2 - 6\hbar$) is the same as in our calculations. However, the middle part of band B (spins $I = 8 - 14\hbar$) is interpreted differently as either proton or neutron $K = 1$ two-quasiparticle bands (in unpaired language they would correspond to either [2,0] or [0,2]). According to our CNS and CRMF calculations, these configurations are more excited (by more than 1 MeV in CNS and by few MeV in CRMF) than the [2,2] configuration with negative γ -deformation and thus should not be assigned to the $I = 8 - 14\hbar$ branch of band B. CNS and CRMF calculations also show that in the spin range $I = 10 - 14\hbar$ the configuration [1,1] is somewhat lower in energy than [2,2]. However, we deem this very unlikely.

The complex version of the Excited Vampir variational approach which includes neutron-proton pairing has been applied for the study of the even-spin positive parity ^{68}Se spectra up to $I = 16^+$ in Ref. [26]. A good description of the energies has been obtained by adjusting several parameters. In particular, the isoscalar spin 0 and 1 particle-particle matrix elements were enhanced and all diagonal $T=0$ monopole matrix elements were shifted. This shift turns out to be important for reproducing the prolate-oblate energy difference, which is obtained in the CRHB+LN calculations without any adjustable parameters. These calculations interpret band C and bottom part of band B similar to us, but the interpretation of top part of band B (spins $I = 8 - 14\hbar$) is different. It remains to be seen whether configurations corresponding to the highly-deformed negative- γ minimum have to be included in the Excited Vampir calculations and in projected shell model for a correct interpretation of this part of band B.

Our interpretation could be corroborated by measurements of transition quadrupole moments Q_t . According to the CRHB+LN calculations, band C and the low-spin part of band B ($I = 2 - 6\hbar$) have average values of $Q_t \approx 1.75$ eb and 1.65 eb, respectively, which are slightly increasing with spin. The $I = 8 - 14\hbar$ part of band B is characterized by quite large values of $Q_t \approx 2.65$ eb [CRMF] and $Q_t \approx 3.05$ eb [CNS], if it is associated with negative- γ

$[2, 2](\alpha = 0)$ configuration. If this branch, however, has the $[1, 1]$ structure, then the CRMF calculations give $Q_t \approx 1.4$ eb. For band A, CRMF predicts that the Q_t values decrease from 1.4 eb at $I = 16\hbar$ to 0.95 eb at $I = 26\hbar$. On the other hand, CNS predicts a decrease from 1.3 eb at $I = 16\hbar$ to 0.8 eb at $I = 22\hbar$.

C. ^{72}Kr

The alleged delay of the crossing between the g-band and the doubly aligned S-band in ^{72}Kr has been in the focus of considerations relating it to the np -pairing. Thereby it was assumed that the high spin part of band B (in the notation of Ref. [49]) represents the doubly aligned S-band (see Ref. [43] and references therein). The rational was that the mean-field calculations predicted this crossing at about the same frequency as in the adjacent isotopes with $N=74$ and 76 , whereas band B shows only a gentle upbend at a substantially higher frequency. However the situation changed with the observation of a second even spin band (band A) of positive parity in Refs. [53,54], which was then confirmed in Ref. [49]. The only difference between these studies is the energy of the $(26^+) \rightarrow (24^+)$ transition. In Refs. [53,54] it has an energy of (2837) keV, while Ref. [49] suggests an energy of (3063) keV and assigns the 2834 keV line (which is very close to 2837 keV transition of Ref. [53,54]) to the link between bands A and B. In the present manuscript, we follow the level scheme of Ref. [49].

The $[2,2]$ and $[3,3]$ configurations are the lowest ($\pi = +, \alpha = 0$) states according to the CNS and CRMF calculations (Fig. 14). The transition quadrupole moments Q_t and the equilibrium deformations of these configurations differ considerably (Fig. 15). We assign the configuration $[2,2]$ to band A. Fig. 14 demonstrates that the $(E - E_{RLD})$ curves of band A and band B (at $I \geq 20\hbar$) and their relative energies are well reproduced by the $[2,2]$ and $[3,3]$ configurations in the CNS calculations. The same holds for the CRMF, which is not shown here since the results are too similar to the CNS. The kinematic moment of inertia of band A above the band crossing is excellently described by the CRMF and CRHB+LN calculations (Fig. 7a). The low spin part of band B is interpreted as the g-band at prolate shape. It is well described by the CRHB+LN calculations in the prolate minimum. Band C is the ground state band in the oblate minimum. In the CRHB+LN calculations for $I = 0\hbar$, the oblate minimum is 1.15 MeV below the prolate one, while in experiment it is ≈ 0.6 MeV [49] lower. The prolate minimum takes over at $I = 4\hbar$, because it has a larger moment of inertia.

In experiment, the g-band (band B: $I = 4 - 14\hbar$) is crossed by the S-band (band A: $I = 16 - 26\hbar$) at $\omega \approx 0.69$ MeV. This value is very close to the crossing frequencies in $^{74,76}\text{Kr}$ which are approximately equal to 0.68 and 0.65 MeV, respectively. Thus recent experimental data do not show the delay of the band crossing in the $N = Z$ system as compared with $N = Z + 2$ system. The CRHB+LN calculations place the band crossing in ^{72}Kr at $\omega \approx 0.53$ MeV (Fig. 7a), i.e. experimental band crossing is by 160 keV delayed as compared with the CRHB+LN calculations, which reproduce very well the crossing frequencies in $^{74,76}\text{Kr}$ (Fig. 7b and c). However, we do not consider this discrepancy as an evidence for $t = 0$ np -pairing, because comparable or even larger differences between calculated and experimental crossing frequencies are known for nuclei in which np -pairing does not play a role (see Sect. V for details).

Having the structure of the g- and S-bands established, we discuss in detail the structure of band B in the spin range $I = 16 - 26\hbar$. First we focus on high spin, where the calculations with zero pairing apply. The CNS calculations indicate the presence of two closely lying [3,3] configurations (Fig. 14), which are candidates for the high-spin branch of band B. The configurations [3,3]a and [3,3]b are obtained from the [2,2] configuration by exciting a proton and a neutron from the $3_3(\alpha = -1/2)$ and $3_3(\alpha = +1/2)$ orbitals into second $g_{9/2}(\alpha = +1/2)$ orbital, respectively. The results of the CRMF calculations for the [2,2] and [3,3]a,b configurations are very similar to those shown in Fig. 14a. The relative energies of the [2,2] and [3,3]a,b configurations depend on the energy gap between the 3_3 and $g_{9/2}$ orbitals, which, as we know from $^{73,74}\text{Kr}$ (see Sect. III A, III B), is well described by the CNS and CRMF calculations. Thus, the fact that for $I \geq 20\hbar$ the experimental energy difference between the top branch of band B and band A comes very close to the calculated one strongly supports the interpretation of top branch of band B as the [3,3] configuration. The details of the interpretation are, however, model dependent. The CNS calculations with the 'A80' set and the CRMF calculations suggest that the top branch of band B may be the envelope of the [3,3]a and [3,3]b configurations, whereas the CNS calculations with the standard Nilsson parameters suggests the [3,3]a configuration. In the former case the irregularities seen in $J^{(2)}$ of the band B at $\omega \geq 0.8$ MeV (see Fig. 2 in Ref. [43]) can be explained as due to the crossing of the [3,3]a and [3,3]b configurations.

Further insight into the structure of the top branch of band B can be obtained by comparing it with negative parity bands 1 and 2 in ^{73}Kr [38] which are based on the [3,3] configurations (see Fig. 16a). These configurations well account for the properties of bands 1 and 2 in ^{73}Kr at $\omega \geq 1.0$ MeV (Fig. 7 in Ref. [38]), while the paired analogs of these configurations (three-quasiparticle configurations $[\pi(3)g_{9/2} \otimes \nu g_{9/2}]$) provide very good description of these bands within the TRS model also below a gradual alignment seen at $\omega \sim 1.0$ MeV (Fig. 8 in Ref. [38]). As compared with the [3,3] configurations in ^{73}Kr , the [3,3] configurations in ^{72}Kr have an additional neutron hole in $3_3(\alpha = \pm 1/2)$. The unpaired configuration [3,3] assigned to band B corresponds the four-quasiparticle $[\pi(3)g_{9/2} \otimes \nu(3)g_{9/2}]$ configuration. Unfortunately, we are not yet able to study this configuration within the CRHB+LN formalism.

Comparing the [3,3] configurations and the top branch of band B (Fig. 16b) suggests that at frequencies higher than the observed ones the aligned angular momentum of the top branch of band B cannot be built in the same way as at lower frequencies, because it will exceed the value allowed by the [3,3] configurations. Thus the slope of the I_x versus ω curve is expected to change around $\omega \sim 1.1$ MeV. This is similar to what is seen at $\omega \sim 1.0$ MeV in the bands 1 and 2 of ^{73}Kr . An extension of the band B to higher spin is required in order to check that.

The calculated deformation parameters of the discussed configurations are shown in Fig. 15. While some differences between the CNS and CRMF results exist, the general features are similar. All the configurations show a gradual decrease of the transition quadrupole moments Q_t (Fig. 15a), which is caused by a decrease of β and an increase of γ . Both in the CNS and CRMF approaches, the [3,3]b configuration jumps from negative to positive γ values at $I \sim 18\hbar$ (Fig. 15c). If this configuration is assigned to the top branch of band B, the jump may cause the irregularities of dynamic moment of inertia seen in experiment (see Fig. 2 in Ref. [43]). The low spin branch of the CRHB+LN results gives the Q_t values for the

g-band, which are close to experimental value [55]. The high spin branch of the CRHB+LN results gives the Q_t values for band A. As seen, neither of the calculations (CRHB+LN, CNS and CRMF for the [2,2] configuration) can explain low experimental value of Q_t for the $I = 22\hbar$ state of band A reported in Ref. [49]. New measurements of transition quadrupole moments in ^{72}Kr are needed in order to confirm or reject this discrepancy.

According to the CNS calculations, there is a non-collective aligned state with [2,2] configuration and $I = 16^+$, which lies ≈ 1.2 MeV below the $I = 16^+$ state of band A. It might be that the third observed state with $I = 16^+$ at $E = 8529$ keV (see Fig. 1 in Ref. [49]) is this aligned state. However, in experiment it lies only 218 keV below the $I = 16^+$ state of band A.

D. ^{76}Sr

In CRMF and CNS calculations without pairing the $(\pi = +, \alpha = 0)$ yrast line in the spin range $I = 0 - 30\hbar$ is dominated by the collective near-prolate [4,4] configuration (Fig. 18a). This is in contrast to neighbouring ^{78}Sr and ^{80}Zr nuclei (Sects. III E and IV E), in which the low-spin near-prolate ground state band is crossed at $I \sim 15 - 20\hbar$ by the band with negative γ -deformation. This difference is due to the large $N = Z = 38$ deformed shell gap at prolate shape (see, for example, the Nilsson diagram in Fig. 8 of Ref. [40]). In the CNS calculations, the [4,4] configuration shows a gradual decrease of the transition quadrupole moment from $Q_t \approx 3.3$ eb ($\varepsilon_2 \approx 0.34$, $\gamma = -3^\circ$) at $I = 16\hbar$ down to $Q_t \approx 2.7$ eb ($\varepsilon_2 \approx 0.32$, $\gamma \approx -1^\circ$) at $I = 26\hbar$.

As seen in Fig. 18, most of the yrast line is well reproduced by the CRHB+LN calculations. Branches A and B shown in this figure are the lowest in energy solutions before and after band crossing. The calculation gives a sharp band crossing at $\omega \approx 0.73$ MeV, whereas the experiment shows a more gradual alignment. This discrepancy may be attributed to the cranking approximation, which is not reliable in the region of the band crossing. The deformation of branch A is almost spin-independent corresponding to $Q_t \approx 3.6$ eb and $\gamma \approx 0^\circ$. The branch B is a paired analog of the [4,4] configuration with $Q_t \approx 2.75$ eb and $\gamma = -5^\circ$ at $I = 20\hbar$ and $Q_t \approx 2.6$ eb and $\gamma = -4^\circ$ at $I = 26\hbar$. Somewhat larger Q_t values ($Q_t \approx 3.16$ eb at $I = 20\hbar$ and $Q_t \approx 2.8$ eb at $I = 26\hbar$) and somewhat smaller γ -deformations ($\gamma \approx -2.5^\circ$) have been obtained for the [4,4] configuration in the CRMF calculations.

The dynamic moments of inertia of the positive parity bands in $^{76,78}\text{Sr}$ and one-quasiparticle bands in ^{77}Sr are compared in Fig. 17. The band crossing in the $N = Z$ nucleus ^{76}Sr occurs at about the same frequency as for the $(\pi = +, \alpha = \pm 1/2)$ and $(\pi = -, \alpha = +1/2)$ bands in ^{77}Sr . The small differences may be caused by polarizations of the deformed potential and of $t = 1$ pair field induced by the additional neutron in ^{77}Sr . The comparison with the yrast sequence in ^{78}Sr is inconclusive, because no clear bandcrossing can be seen (see Sect. III E for detail).

E. ^{80}Zr

According to the unpaired CRMF and CNS calculations, the near-prolate [6,6] configuration forms the ($\pi = +, \alpha = 0$) yrast line at low spin. At $I \approx 10\hbar$ it is crossed by the [4,4] configuration with $\gamma \sim -30^\circ$ (Fig. 19a), which is the energetically favored collective configuration in the spin range $I = 10 - 28\hbar$. The paired analogs in the CRHB+LN calculations are the configurations denoted by A and B, respectively. Branch A is in good agreement with the experimental energies and moments of inertia (Fig. 19). The experimentally observed spins remain below the predicted band crossing. These two collective configurations dominate the yrast line. According to the CNS calculations, only at spins $I = 16, 22, 24\hbar$ (and at $I = 26\hbar$ with the standard Nilsson parameters), the aligned or weakly collective ($I = 22\hbar$) states of the [2,2] and [3,3] configurations are lower in energy than the [4,4] configuration.

In all unpaired calculations, the [6,6] configuration has $Q_t \approx 3.9 \text{ eb}$, $\varepsilon_2 \approx 0.38$ and $\gamma \approx -1^\circ$, which stay nearly constant in the spin range $I = 0\hbar - 18\hbar$. In the CNS calculation with the 'A80' Nilsson parameters, the [4,4] configuration shows a gradual decrease of the quadrupole moment from $Q_t = 3.45 \text{ eb}$ ($\varepsilon_2 = 0.31, \gamma = -34^\circ$) at $I = 10\hbar$ to $Q_t = 2.39 \text{ eb}$ ($\varepsilon_2 = 0.22, \gamma = -25^\circ$) at $I = 28\hbar$. For the CNS calculations with the standard Nilsson parameters we find a decrease from $Q_t = 3.66 \text{ eb}$ ($\varepsilon_2 = 0.32, \gamma = -37^\circ$) at $I = 10\hbar$ to $Q_t = 2.88 \text{ eb}$ ($\varepsilon_2 = 0.26, \gamma = -33^\circ$) at $I = 28\hbar$. In the CRMF calculations for this configurations Q_t drops from 2.9 eb ($\gamma = -24^\circ$) to 2.1 eb ($\gamma = -24^\circ$) in the same spin range. The deformation of the [4,4] configuration depends stronger on the model and the parametrization. The influence of pairing on the deformation of the configurations A and B (paired analogs of the [6,6] and [4,4] configurations) is rather marginal, while the excitation energies, and, consequently, the moments of inertia change stronger (see Fig. 19).

V. IS THERE EVIDENCE FOR AN ISOSCALAR NP -PAIR FIELD?

In a number of publications it has been suggested that rotational properties of the $N \approx Z$ nuclei can provide evidence for the presence of a $t = 0$ np pair field. However, the reasoning often ignored the considerable β - and γ -softness of the nuclei in the mass region of interest. In this section we are going to discuss if the comparison of the data available at present with our calculations, which assume a realistic (not only monopole) $t = 1$ pair field and take the shape changes into account, suggests any evidence for the existence of a $t = 0$ np pair field. The size of the moment of inertia, the frequencies at which the pairs of particles align their angular momentum (band crossing frequencies), and unexpected mixing of configurations with a different number of quasiparticles have been discussed in the literature as possible indicators of np -pairing in rotating $N \approx Z$ nuclei.

A. Moments of inertia

Since $t = 0$ pairs carry angular momentum, a $t = 0$ np -pair field is expected to increase the moment of inertia [34,56–58]. In contrast to the $t = 1$ pair field, which is suppressed by the Coriolis anti-pairing (CAP) effect, $t = 0$ np -pairing is favored by rotation. Thus, at large angular momentum, where the $t = 1$ field is destroyed, a substantial difference

between experimental and calculated moments of inertia may indicate the presence of the $t = 0$ np -pair field.

The moments of inertia in the g-bands of all $N = Z$ nuclei are well reproduced by our calculations. In particular this is true for ^{80}Zr . For this nucleus Ref. [58] carried out Cranked Hartree-Fock Bogoliubov calculation that included both $t = 0$ and $t = 1$ np -pair fields. A transition from dominating $t = 1$ pairing to dominating $t = 0$ pairing was found for the yrast line, which contained a spin region where both pair fields coexist. However, the calculated kinematic moment of inertia increased from $J^{(1)} \approx 10 \text{ MeV}^{-1}$ at $\omega \sim 0.2 \text{ MeV}$ to $J^{(1)} \approx 40 \text{ MeV}^{-1}$ at $\omega \sim 0.3 \text{ MeV}$ (see Fig. 12 in Ref. [58]), which is in discrepancy with experiment.

Our calculations as well as the ones in Ref. [57] indicate that after first proton and neutron paired band crossings the static $t = 1$ pairing correlations are essentially gone. In this regime of fast rotation, the calculations without pairing provide very good description of the rotational properties of different types of bands (terminating, superdeformed etc.) in different regions of the periodic table (see Refs. [12,15,18]). In accordance with this general observation, the experimental moments of inertia in the $N = Z$ nuclei (see present manuscript for ^{68}Se , ^{72}Kr , ^{76}Se and ^{80}Zr nuclei and Refs. [9,17,18,50] for ^{58}Cu , ^{60}Zn , ^{70}Br and ^{74}Rb nuclei) and in the $N = Z + 1$ nuclei (see Refs. [38] [^{73}Kr] and [19] [^{59}Cu]) above the first neutron and/or proton paired band crossings are well reproduced by the unpaired CNS and CRMF calculations, where it turned out to be important that the response of the nuclear shape to rotation was properly taken into account. No systematic underestimate of the moments of inertia, which could be taken as an evidence for a $t = 0$ np -pair field, could be identified.

B. Delayed band crossings

A delay of the first band crossing in the ground state band of an even-even $N = Z$ system has been widely discussed as an evidence for $t = 0$ pair correlations [59,60]. HFB calculations [59] and shell model calculations [60] in a $f_{7/2}$ subshell at fixed deformation indicate that the increase of the value of the $t = 0$ np -pair strength results in a delay of the crossing frequency in the ground state band of $N = Z$ even-even nuclei. CSM investigations [27,61,62] show that such a delay can also be caused by the $t = 1$ np -pairing.

As discussed in Sect. IV C, the experimental situation in ^{72}Kr turned out to be more complex than originally anticipated. According to recent data the crossing of the g- and S-bands takes place at approximately the same frequency as in $^{74,76}\text{Kr}$. No delay of band crossing is seen in ^{68}Se as compared with ^{70}Se (see Ref. [49]). As discussed in Sects. IV D and III E, the comparison of the experimental crossing frequencies in ^{76}Sr and ^{78}Sr is not conclusive. There are no data permitting a comparison for ^{80}Zr . Our CRHB+LN calculations give a crossing frequency that is close to experimental data. Only for ^{72}Kr the calculations underestimate it by 160 keV.

A number of unexplained delays of the band crossing frequency as compared with the predictions of the CSM models has been observed in regions away from the $N = Z$ line (see below), where they cannot be attributed to the np -pairing. The polarization effects at the band crossing (deformation changes, current changes etc.) are dramatic in the soft $A = 60 - 80$ nuclei. With this in mind we conclude that no systematic delay of the crossing between the g-band and the doubly aligned S-band as compared to our CRHB+LN calculations has

been found. Previous studies that correlate the delay of the band crossing frequencies with the effects of the np -pairing should be treated with considerable caution. They should be verified in the cranked mean field models which take these polarization effects into account in a more self-consistent way.

Let us mention two examples of delayed band crossings in nuclei, where np -pairing is not expected to play a role. The $\nu h_{11/2}$ crossings in the ground state bands of the even-even Nd ($Z = 60$) and Ce ($Z = 58$) nuclei with $A \sim 130$ (see Ref. [63] and references therein) are considerably delayed, where the maximum of this delay is situated around $N = 70$ and $Z = 58 - 60$. While the CSM model with the deformations taken from the TRS calculations predicts more or less constant value of crossing frequency as a function of neutron number, the experiment shows large variations in crossing frequencies being in the case of ^{132}Nd in close agreement with calculations, while in other cases exceeding the CSM predictions by up to 55 %. Similar delays are also seen in odd Nd and Ce nuclei and odd and odd-odd La ($Z = 57$) and Pr ($Z = 59$) nuclei [63]. In contrast, the $\pi h_{11/2}$ crossings are well reproduced by the CSM. Although predicted triaxial softness of heaviest nuclei may be responsible for this delay, no clear supporting evidence for that exists now [63]. Delays of band crossings were observed also in the ground state bands of some rare-earth nuclei with $A \approx 180$. For example, the crossing in the ground state band is delayed in $^{180,182}\text{Hf}$ nuclei as compared with lower mass isotopes [64]. It was suggested in the framework of the projected shell model that such delays are due to quadrupole pairing [65]. However, this is not supported by the CRHB+LN calculations which employ the Gogny force in pairing channel, and, thus, include all multipole interactions. For example, these calculations reproduce well the band crossing frequencies in $^{172,178}\text{Hf}$, but fail to reproduce the delay of the band crossing in ^{180}Hf .

C. Mixing of [2,2] and [3,3] configurations

Due to the Pauli principle, the $t = 1$ pair field cannot scatter np pairs in identical orbitals. Only $t = 0$ np pairs can be in identical states and be scattered. Therefore, strong mixing of configurations which differ by a change of such $t = 0$ np pair may be an evidence for $t = 0$ pair correlations. However, it has to be mentioned, that this is not necessarily evidence for the presence of a $t = 0$ pair field, because a finite matrix element of the residual interaction can cause a substantial mixing of two configurations with close energies.

This type of configuration mixing has first been discussed for ^{73}Kr [38]. It was speculated that in bands 2 and 3 at intermediate spin the configuration changes from $(\pi g_{9/2}^2 \otimes \nu(fp)g_{9/2}^2)$ to $(\pi(fp)g_{9/2} \otimes \nu(fp)g_{9/2}^2)$, which corresponds to a transfer of a neutron-proton pair from the pf orbital into the $g_{9/2}$ orbital.

In ^{70}Br and ^{72}Kr , the [2,2] and [3,3] configurations are located very close in energy (see Fig. 14 in Ref. [50] and Fig. 14 in the present manuscript). If the $t = 0$ np -pairing is present, these configurations are expected to be mixed. A mixing represents the scattering of a proton and neutron on identical negative parity $N = 3$ orbitals into identical $g_{9/2}$ orbitals, and vice versa. Such a pair has an isospin $t = 0$, since the proton and neutron are in the same space-spin state. It was speculated in Sect. VID of Ref. [50] that the observation of one smooth rotational band HD1 in ^{70}Br at high spin instead of the calculated distinct crossing between the [2,2] and [3,3] configurations at $I \sim 18\hbar$ may point to a such mixing.

More detailed experimental investigation of spectra in ${}^{70}\text{Br}$ in the spin range $I = 10 - 30\hbar$ (and, in particular, the observation of the bands associated with the [2,2] configurations) is needed to clarify the situation in this nucleus. In particular, a determination of Q_t for band HB1 via lifetime measurements could clarify the situation, since the calculated Q_t is twice as large for the [3,3] ($\gamma \sim -20^\circ$) configuration as for the [2,2] configurations (see insert in Fig. 6).

In ${}^{72}\text{Kr}$, the high spin branch of band B is assigned to the [3,3] configuration. Band B is the g-band at low spin, which is a superposition of the configurations [2,2] and [4,4]. This means that band B changes from this structure at low spin to [3,3] at medium/high spin. This change proceeds in a reasonably smooth way (Fig. 14). It is possible that the peak in the dynamical moment of inertia seen at 0.85 MeV (see Fig. 2 in Ref. [43]) reflects this change. The smooth transition from the [2,2]+[4,4] structure at low spin to [3,3] at high spin would indicate a scattering of $t = 0$ np pairs. However, this explanation implies that there should also be such scattering between bands B and A, which are assigned to [3,3] and [2,2] configurations, respectively. The scattering should shift the levels of band A and lead to the modifications of the dynamic moment of inertia at these frequencies, which is, however, smooth in experiment. Also the small distance of the $I = 16^+$ states of bands A and B speaks against a strong interaction between the two bands. However, for a final judgment one has to carry a three-band (g, [2,2], [3,3]) mixing analysis.

The discussed band mixings might be interpreted as related to the scattering of np pairs on identical single-particle states in the $N = 3$ shell and the $g_{9/2}$ shell. However we do not consider this as sufficient evidence for the presence of a $t = 0$ pair field. Rather it may indicate weak dynamical $t = 0$ pair correlations as suggested by the Monte Carlo shell model calculations [3] or just mixing of energetically close configurations by residual interaction.

VI. CONCLUSIONS

The rotational bands in even-even $N \approx Z$ nuclei have been studied by means of the cranked Nilsson+Strutinsky approach, cranked relativistic mean field and cranked relativistic Hartree+Bogoliubov theories. Due to the spontaneous breaking of the isospin symmetry by the isovector pair field, its np component needs not to be taken into account explicitly. It is included implicitly when the isospin symmetry is restored by adding the isorotational energy $T(T + 1)/2J_{iso}$ to the intrinsic energy [27]. Since $T = 1$ states lie at a substantial excitation energy in even-even $N = Z$ nuclei, only $T = 0$ rotational bands were considered, which means that the isorotational energy shift is irrelevant for the rotational response. The systematic investigation of the rotating even-even $N = Z$ nuclei with $A = 68 - 80$ leads to the following conclusions.

Coexistence of prolate and oblate shapes is found near the ground state. For $I > 2$, the yrast states have prolate shape. Their moments of inertia are well reproduced by the calculations that take only the isovector pair field into account. At high spin, the isovector pairing is very weak and calculations with zero pairing agree well with the results of treating the isovector pairing in the framework of the Lipkin-Nogami approximation. All these calculations account well for the data. This concerns the moments of inertia as well as the relative energies of different configurations. The level of agreement between theory and experiment is comparable, sometimes even better than for the nuclei away from the $N = Z$

line. The available experimental high-spin data do not require the introduction of the $t = 0$ np -pairing into the models, and, thus, do not provide any evidence of this type of pairing.

The delay of the crossing between the ground band and the doubly aligned S-band in even-even $N = Z$ nuclei has been suggested as an evidence for the $t = 0$ [34,59] np pair field. The new data do not show such a delay in ^{72}Kr , which was considered as the most important evidence. Such delay is also absent in ^{68}Se [49]. The data on other even-even nuclei do not permit us to compare the band crossing frequencies in $N = Z$ and $N = Z + 2$ isotopes. The properties of bands in paired regime and the paired band crossings in ^{68}Se (Sect. IV B), ^{72}Kr (Sect. IV C), ^{76}Sr (Sect. IV D) and ^{80}Zr (Sect. IV E) are reasonably well described by the CRHB+LN theory (which implicitly takes into account the isovector np -pairing). The minor differences between experimental and calculated band crossing frequencies are within the expected accuracy of our theoretical tools.

There seems to be strong mixing between some configurations that are related to each other by the transfer of a $t = 0$ np pair on identical single particle states, which may be caused by $t = 0$ np pair correlations. However, this cannot be considered as sufficient evidence for the presence of a $t = 0$ pair field.

The systematic analysis of the rotational response of even-even $N = Z$ nuclei confirms the picture suggested in Ref. [27]. At low spin, there is no isoscalar np pair field but a strong isovector pair field exists, which includes a large np component, the strength of which is determined by isospin conservation. Like in nuclei away from the $N = Z$ line, this isovector pair field is destroyed by rotation. In this high spin regime calculations without pairing describe well the data provided the drastic shape changes that cause among other things band termination are taken into account.

VII. ACKNOWLEDGEMENTS

We thank Carl Svensson for providing and allowing us to use recent unpublished experimental data on ^{74}Kr . The work was supported by the DoE grant DE-F05-96ER-40983.

REFERENCES

- [1] J. Engel, K. Langanke, and P. Vogel, Phys. Lett. B **389**, 211 (1996).
- [2] J. Engel, S. Pittel, M. Stoitsov, P. Vogel, and J. Dukelsky, Phys. Rev. C **55**, 1781 (1997).
- [3] D. J. Dean, S. E. Koonin, K. Langanke and P. B. Radha, Phys. Lett. B **399**, 1 (1997).
- [4] D. R. Bes, R. A. Broglia, O. Hansen, O. Nathan, Phys. Rep. **34**, 1 (1977).
- [5] A. O. Macchiavelli, P. Fallon, R. M. Clark, M. Cromaz, M. A. Deleplanque, R. M. Diamond, G. J. Lane, I. Y. Lee, F. S. Stephens, C. E. Svensson, K. Vetter, and D. Ward, Phys. Lett. B **480**, 1 (2000).
- [6] J. Jänecke, Nucl. Phys. **73**, 97 (1965).
- [7] P. Vogel, Nucl. Phys. **A662**, 148 (2000).
- [8] A. O. Macchiavelli, P. Fallon, R. M. Clark, M. Cromaz, M. A. Deleplanque, R. M. Diamond, G. J. Lane, I. Y. Lee, F. S. Stephens, C. E. Svensson, K. Vetter, and D. Ward, Phys. Rev. C **61**, 041303(R) (2000).
- [9] C. D. O'Leary, C. E. Svensson, S. G. Frauendorf, A. V. Afanasjev, D. E. Appelbe, R. A. E. Austin, G. C. Ball, J. A. Cameron, R. M. Clark, M. Cromaz, P. Fallon, D. F. Hodgson, N. S. Kelsall, A. O. Macchiavelli, I. Ragnarsson, D. Sarantites, J. C. Waddington and R. Wadsworth, Phys. Rev. C **67**, 021301(R) (2003).
- [10] T. Bengtsson and I. Ragnarsson, Nucl. Phys. **A436**, 14 (1985).
- [11] A. V. Afanasjev and I. Ragnarsson, Nucl. Phys. **A591**, 387 (1995).
- [12] A. V. Afanasjev, D. B. Fossan, G. J. Lane and I. Ragnarsson, Phys. Rep. **322**, 1 (1999).
- [13] W. Koepf and P. Ring, Nucl. Phys. **A493**, 61 (1989).
- [14] J. König and P. Ring, Phys. Rev. Lett. **71**, 3079 (1993).
- [15] A. V. Afanasjev, J. König and P. Ring, Nucl. Phys. **A608**, 107 (1996).
- [16] A. V. Afanasjev, P. Ring, and J. König, Nucl. Phys. **A676**, 196 (2000).
- [17] C. E. Svensson, D. Rudolph, C. Baktash, M. A. Bentley, J. A. Cameron, M. P. Carpenter, M. Devlin, J. Eberth, S. Flibotte, A. Galindo-Uribarri, G. Hackman, D. S. Haslip, R. V. F. Janssens, D. R. LaFosse, T. J. Lampman, I. Y. Lee, F. Lerma, A. O. Macchiavelli, J. M. Nieminen, S. D. Paul, D. C. Radford, P. Reiter, L. L. Riedinger, D. G. Sarantites, B. Schaly, D. Seweryniak, O. Thelen, H. G. Thomas, J. C. Waddington, D. Ward, W. Weintraub, J. N. Wilson, C. H. Yu, A. V. Afanasjev, and I. Ragnarsson, Phys. Rev. Lett. **82**, 3400 (1999).
- [18] A. V. Afanasjev, I. Ragnarsson and P. Ring, Phys. Rev. C **59**, 3166 (1999).
- [19] C. Andreoiu, D. Rudolph, C. E. Svensson, A. V. Afanasjev, J. Dobaczewski, I. Ragnarsson, C. Baktash, J. Eberth, C. Fahlander, D. S. Haslip, D. R. LaFosse, S. D. Paul, D. G. Sarantites, H. G. Thomas, J. C. Waddington, W. Weintraub, J. N. Wilsson and C.-H. Yu, Phys. Rev. C **62**, 051301(R) (2000).
- [20] A. V. Afanasjev, J. König, P. Ring, L. M. Robledo, and J. L. Egido, Phys. Rev. C **62**, 054306 (2000).
- [21] A. V. Afanasjev, T. L. Khoo, S. Frauendorf, G. A. Lalazissis, and I. Ahmad, Phys. Rev. C **67**, 024309 (2003).
- [22] A. V. Afanasjev, J. König, and P. Ring, Phys. Rev. C **60**, 051303 (1999).
- [23] D. Vretenar, A. V. Afanasjev, G. Lalazissis, and P. Ring, submitted to Physics Reports
- [24] R. A. Wyss and W. Satuła, Acta Phys. Polonica B **32**, 2457 (2001).
- [25] Y. Sun, Eur. Phys. Jour. **20**, 133 (2004).
- [26] A. Petrovici, K. W. Schmid, and A. Faessler, Nucl. Phys. **A 710**, 246 (2002).

- [27] S. G. Frauendorf and J. A. Sheikh, Nucl. Phys. **A645**, 509 (1999).
- [28] G. A. Lalazissis, J. König and P. Ring, Phys. Rev. C **55**, 540 (1997).
- [29] J. F. Berger, M. Girod, and D. Gogny, Comp. Phys. Comm. **63**, 365 (1991).
- [30] D. Galeriu, D. Bucurescu, and M. Ivašku, J. Phys. G **12**, 329 (1986).
- [31] W. Nazarewicz, J. Dudek, R. Bengtsson, T. Bengtsson, and I. Ragnarsson, Nucl. Phys. **A435**, 397 (1985).
- [32] C. E. Svensson, C. Baktash, G. C. Ball, J. A. Cameron, M. Devlin, J. Eberth, S. Flibotte, A. Galindo-Uribarri, D. S. Haslip, V. P. Janzen, D. R. LaFosse, I. Y. Lee, A. O. Macchiavelli, R. W. MacLeod, J. M. Nieminen, S. D. Paul, D. C. Radford, L. L. Riedinger, D. Rudolph, D. G. Sarantites, H. G. Thomas, J. C. Waddington, D. Ward, W. Weintraub, J. N. Wilson, A. V. Afanasjev and I. Ragnarsson, Phys. Rev. Lett. **80**, 2558 (1998).
- [33] C. Plettner, H. Schnare, R. Schwengner, L. Käubler, F. Dönau, I. Ragnarsson, A. V. Afanasjev, A. Algora, G. de Angelis, A. Gadea, D. R. Napoli, J. Eberth, T. Steinhardt, O. Thelen, M. Hausmann, A. Müller, A. Jungclaus, K. P. Lieb, D. G. Jenkins, R. Wadsworth, A. N. Wilson and S. Frauendorf, Phys. Rev. C **62**, 014313 (2000).
- [34] S. Satuła and R. Wyss, Phys. Lett. B **393**, 1 (1997).
- [35] R. Cardona, F. Cristancho, S. L. Tabor, R. A. Kaye, G. Z. Solomon, J. Döring, G. D. Johns, M. Devlin, F. Lerma, D. G. Sarantites, I.-Y. Lee, A. O. Macchiavelli, I. Ragnarsson, Phys. Rev. C **68**, 024303 (2003).
- [36] C. E. Svensson, private communication (2003).
- [37] S. Balraj, Nucl. Data Sheets **74**, 63 (1995); C. E. Svensson, C. D. O'Leary, I. Ragnarsson, D. E. Appelbe, R. A. E. Austin, G. C. Ball, J. A. Cameron, R. M. Clark, M. Cromaz, P. Fallon, D. F. Hodgson, N. S. Kelsall, A. O. Macchiavelli, D. Sarantites, J. C. Waddington, R. Wadsworth, and D. Ward, submitted to Phys. Rev. C
- [38] N. S. Kelsall, S. M. Fischer, D. P. Balamuth, G. C. Ball, M. P. Carpenter, R. M. Clark, J. Durell, P. Fallon, S. J. Freeman, P. A. Hausladen, R. V. F. Janssens, D. G. Jenkins, M. J. Leddy, C. J. Lister, A. O. Macchiavelli, D. G. Sarantites, D. C. Schmidt, D. Seweryniak, C. E. Svensson, B. J. Varley, S. Vincent, R. Wadsworth, A. N. Wilson, A. V. Afanasjev, S. Frauendorf, I. Ragnarsson and R. Wyss, Phys. Rev. C **65**, 044331 (2002).
- [39] A. Algora, G. de Angelis, F. Brandolini, R. Wyss, A. Gadea, E. Farnea, W. Gelletly, S. Lunardi, D. Bazzacco, C. Fahlander, A. Aprahamian, F. Becker, P. G. Bizzetti, A. Bizzetti-Sona, D. de Acuña, M. De Poli, J. Eberth, D. Foltescu, S. M. Lenzi, T. Martinez, D. R. Napoli, P. Pavan, C. M. Petrache, C. Rossi Alvarez, D. Rudolph, B. Rubio, S. Skoda, P. Spolaore, R. Menegazzo, H. G. Thomas, and C. A. Ur, Phys. Rev. C **61**, 031303(R) (2000).
- [40] D. Rudolph, C. Baktash, C. J. Gross, W. Satuła, R. Wyss, I. Birriel, M. Devlin, H.-Q. Jin, D. R. LaFosse, F. Lerma, J. X. Saladin, D. G. Sarantites, G. N. Sylvan, S. L. Tabor, D. F. Winchell, V. Q. Wood, and C. H. Yu, Phys. Rev. C **56**, 98 (1997).
- [41] C. Chandler, P. H. Regan, C. J. Pearson, B. Blank, A. M. Bruce, W. N. Catford, N. Curtis, S. Czajkowski, W. Gelletly, R. Grzywacz, Z. Janas, M. Lewitowicz, C. Marchand, N. A. Orr, R. D. Page, A. Petrovici, A. T. Reed, M. G. Saint-Laurent, S. M. Vincent, R. Wadsworth, D. D. Warner, and J. S. Winfield, Phys. Rev. C **56**, 2924(R) (1997).
- [42] A. V. Afanasjev, P. Ring and I. Ragnarsson, Proc. Int. Workshop PINGST2000 "Se-

lected topics on $N = Z$ nuclei”, 2000, Lund, Sweden, Eds. D. Rudolph and M. Hellström, (2000) p. 183.

[43] S. M. Fischer, C. J. Lister, D. P. Balamuth, R. Bauer, J. A. Becker, L. A. Bernstein, M. P. Carpenter, J. Durell, N. Fotiades, S. J. Freeman, P. E. Garrett, P. A. Hausladen, R. V. F. Janssens, D. Jenkins, M. Leddy, J. Ressler, J. Schwartz, D. Svelnys, D. G. Sarantites, D. Seweryniak, B. J. Varley, and R. Wyss, Phys. Rev. Lett. **87**, 132501 (2001).

[44] A. Harder, F. Dönau, K. P. Lieb, R. A. Cunningham, W. Gelletly, C. J. Gross, F. Hannachi, M. K. Kabadiyski, H. A. Roth, D. Rudolph, J. Simpson, Ö. Skeppstedt, B. J. Varley, and D. D. Warner, Phys. Lett. B **374**, 277 (1996).

[45] A. Harder, A. Jungclaus, M. K. Kabadiyski, D. Kast, K. P. Lieb, D. Rudolph, M. Weiszflog, T. D. Johnson, G. Winter, C. J. Gross, R. A. Cunningham, W. Gelletly, J. Simpson, D. D. Warner, I. G. Bearden, T. Shizuma, G. Sletten, D. Foltescu, H. A. Roth, Ö. Skeppstedt, and B. J. Varley, Phys. Rev. C **55**, 1680 (1997).

[46] C. J. Gross, C. Baktash, D. M. Cullen, R. A. Cunningham, J. D. Garrett, W. Gelletly, F. Hannachi, A. Harder, M. K. Kabadiyski, K. P. Lieb, C. J. Lister, W. Nazarewicz, H. A. Roth, D. Rudolph, D. G. Sarantites, J. A. Sheikh, J. Simpson, Ö. Skeppstedt, B. J. Varley, and D. D. Warner, Phys. Rev. C **49**, R580 (1994).

[47] A. V. Afanasjev and I. Ragnarsson, unpublished

[48] P. J. Ennis, C. J. Lister, W. Gelletly, H. G. Price, B. J. Varley, P. A. Butler, T. Hoare, S. Ćwiok, W. Nazarewicz, Nucl. Phys. A 535 (1991) 392

[49] S. M. Fischer, C. J. Lister, and D. P. Balamuth, Phys. Rev. C **67**, 064318 (2003).

[50] D. G. Jenkins, N. S. Kelsall, C. J. Lister, D. P. Balamuth, M. P. Carpenter, T. A. Sienko, S. M. Fischer, R. M. Clark, P. Fallon, A. Görzen, A. O. Macchiavelli, C. E. Svensson, R. Wadsworth, W. Reviol, D. G. Sarantites, G. C. Ball, J. Rikovska Stone, O. Juillet, P. van Isacker, A. V. Afanasjev and S. Frauendorf, Phys. Rev. C **65**, 064307 (2002).

[51] S. M. Fischer, D. P. Balamuth, P. A. Hausladen, C. J. Lister, M. P. Carpenter, D. Seweryniak and J. Schwartz, Phys. Rev. Lett. **84**, 4064 (2000).

[52] Y. Sun, Z. Ma, A. Aprahamian, and M. Wiescher, preprint nucl-th/0107004

[53] N. S. Kelsall, C. E. Svensson, S. Fischer, D. E. Appelbe, R. A. E. Austin, D. P. Balamuth, G. C. Ball, J. A. Cameron, M. P. Carpenter, R. M. Clark, M. Cromaz, M. A. Deleplanque, R. M. Diamond, J. L. Durell, P. Fallon, S. J. Freeman, P. A. Hausladen, D. F. Hodgson, R. V. F. Janssens, D. G. Jenkins, G. J. Lane, M. J. Leddy, C. J. Lister, A. O. Macchiavelli, C. D. O’Leary, D. G. Sarantites, F. S. Stephens, D. C. Schmidt, D. Seweryniak, B. J. Varley, S. Vincent, K. Vetter, J. C. Waddington, R. Wadsworth, D. Ward, A. N. Wilson, A. V. Afanasjev, S. Frauendorf, I. Ragnarsson and R. Wyss, Proc. Int. Conf. on “Frontiers of Nuclear Structure”, (Berkeley, California, 2002), AIP Conf. Proc. v. 656, Eds. P. Fallon and R. Clark, (Melville, New York, 2003) p. 261.

[54] N. S. Kelsall, C. E. Svensson, S. Fischer, D. E. Appelbe, R. A. E. Austin, D. P. Balamuth, G. C. Ball, J. A. Cameron, M. P. Carpenter, R. M. Clark, M. Cromaz, M. A. Delaplanque, R. M. Diamond, P. Fallon, D. F. Hodgson, R. V. F. Janssens, D. G. Jenkins, G. J. Lane, C. J. Lister, A. O. Macchiavelli, C. D. O’Leary, D. G. Sarantites, F. S. Stephens, D. C. Schmidt, D. Seweryniak, K. Vetter, J. C. Waddington, R. Wadsworth, D. Ward, A. N. Wilson, A. V. Afanasjev, S. Frauendorf, I. Ragnarsson, Eur. Phys. Jour.

A **20**, 131 (2004).

- [55] G. de Angelis, C. Fahlander, A. Gadea, E. Farnea, W. Gelletly, A. Aprahamian, D. Bazzacco, F. Becker, P. G. Bizzeti, A. Bizzeti-Sona, F. Brandolini, D. de Acuña, M. De Poli, J. Eberth, D. Foltescu, S. M. Lenzi, S. Lunardi, T. Martinez, D. R. Napoli, P. Pavan, C. M. Petrache, C. Rossi Alvarez, D. Rudolph, B. Rubio, W. Satuła, S. Skoda, P. Spolaore, H. G. Thomas, C. A. Ur, and R. Wyss, Phys. Lett. B **415**, 217 (1997).
- [56] E. M. Müller, K. Mühlhans, K. Neergård, U. Mosel, Nucl. Phys. **A383**, 233 (1982).
- [57] S. Satuła and R. Wyss, Nucl. Phys. **A676**, 120 (2000).
- [58] A. L. Goodman, Phys. Rev. C **63**, 044325 (2001).
- [59] J. A. Sheikh and R. Wyss, Phys. Rev. C **62**, 051302(R) (2000).
- [60] N. S. Kelsall, R. Wadsworth, A. N. Wilson, P. Fallon, A. O. Macchiavelli, R. M. Clark, D. G. Sarantites, D. Seweryniak, C. E. Svensson, S. M. Vincent, S. Frauendorf, J. A. Sheikh, and G. C. Ball, Phys. Rev. C **64**, 024309 (2001).
- [61] K. Kaneko and J. Zhang, Phys. Rev. C **57**, 1732 (1998).
- [62] S. Frauendorf and J. A. Sheikh, Phys. Rev. C **59**, 1400 (1999).
- [63] O. Zeidan, D. J. Hartley, L. L. Riedinger, W. Reviol, W. D. Weintraub, Y. Sun, Jing-ye Zhang, A. Galindo-Uribarri, S. D. Paul, D. G. Sarantites, M. Devlin, M. P. Carpenter, R. V. F. Janssens and D. Seweryniak, Phys. Rev. C **66**, 044311 (2002).
- [64] P. Chowdhury *et al.*, to be published.
- [65] Y. Sun, S. Wen and D. H. Feng, Phys. Rev. Lett. **72**, 3483 (1994).

FIGURES

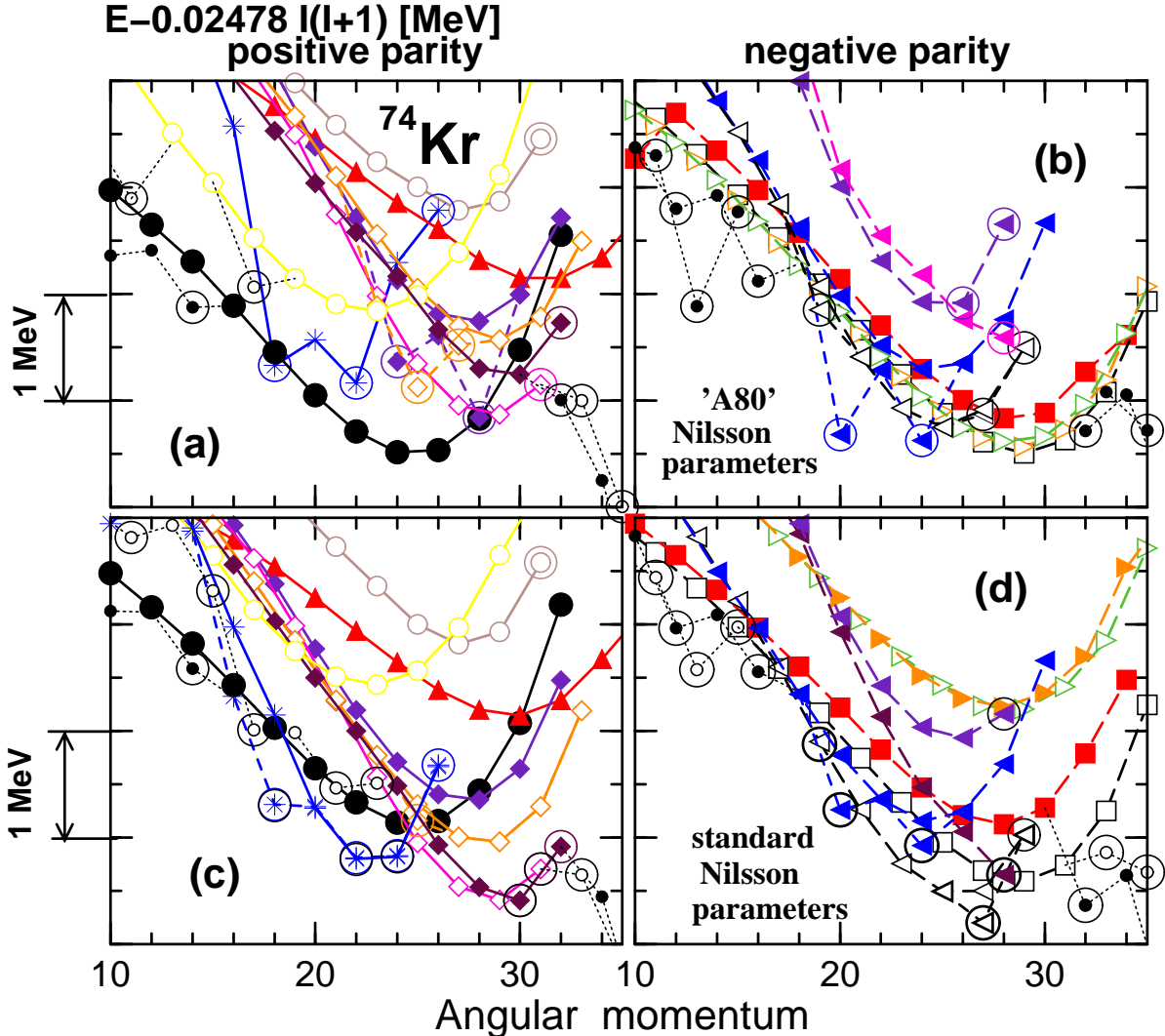


FIG. 1. Excitation energies of the ^{74}Kr configurations relative to a rigid-rotor reference $E_{RLD} = 0.02478I(I + 1)$ MeV obtained within the CNS approach. The standard set of the Nilsson parameters (bottom panels) is compared with the 'A80' set (top panels). Solid and open circles are used for signature $\alpha = 0$ and $\alpha = 1$ states, respectively. Solid and long-dashed lines are used for positive and negative parity states, respectively. Terminating (aligned) states are encircled. The absence of encircling indicates that the band continues beyond the maximum spin, see Refs. [12,18] for details. Short-dashed lines are used to show non-collective and weakly collective branches of configurations. Dotted lines are used for yrast lines at low and high spins. The configurations correspond to the symbols: [2,2] - stars, [2,3] - triangles left, [3,3] - diamonds, [2,4] - circles, [3,4] - squares, [4,4] - triangles up and [(1)3,4] - triangles right.

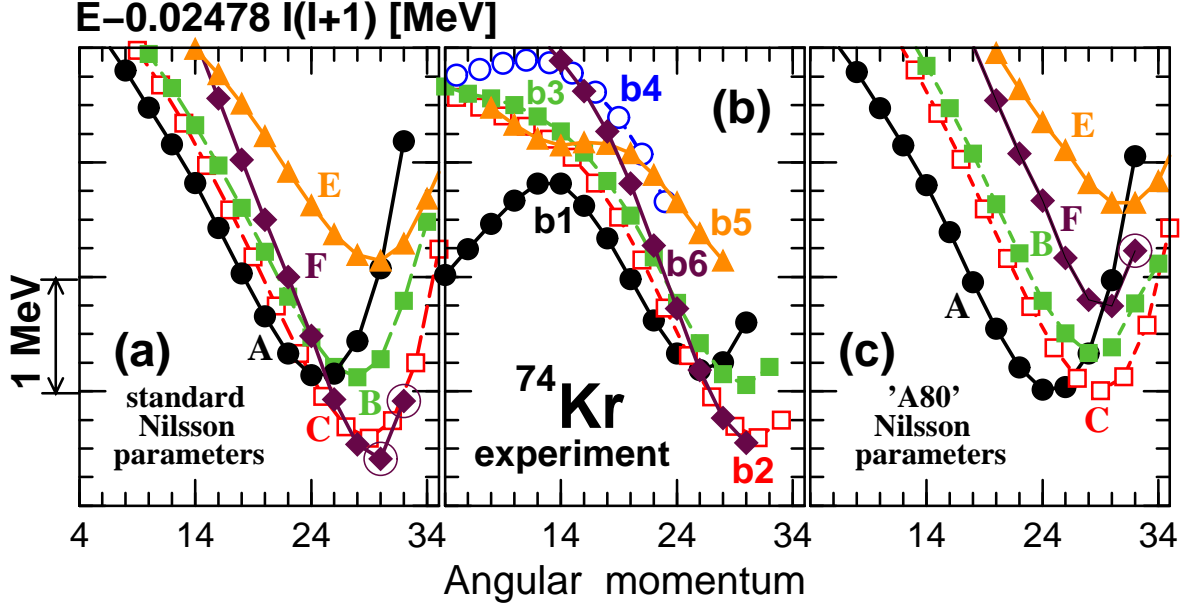


FIG. 2. Excitation energies of the experimental bands 1-6 in ^{74}Kr and the configurations [2,4] (A), [3,4] (B,C), [3,3] (F), and [4,4] (E) calculated in the CNS approach relative to a rigid rotor reference $E_{RLD} = 0.02478I(I + 1)$ MeV. Experimental data are taken from Refs. [36,40]. Note that the lowest state in band 6 is placed at an arbitrary excitation energy of $E_{exc} = 4.9$ MeV and its spin is set to $I^\pi = 8^+$. Solid and dashed lines are used for positive and negative parities, respectively. Solid and open symbols are used for signatures $\alpha = +1/2$ and $\alpha = -1/2$, respectively. In panel (b), solid circles, open squares, solid squares, open circles, solid triangles, diamonds are used for bands 1, 2, 3, 4, 5 and 6, respectively.

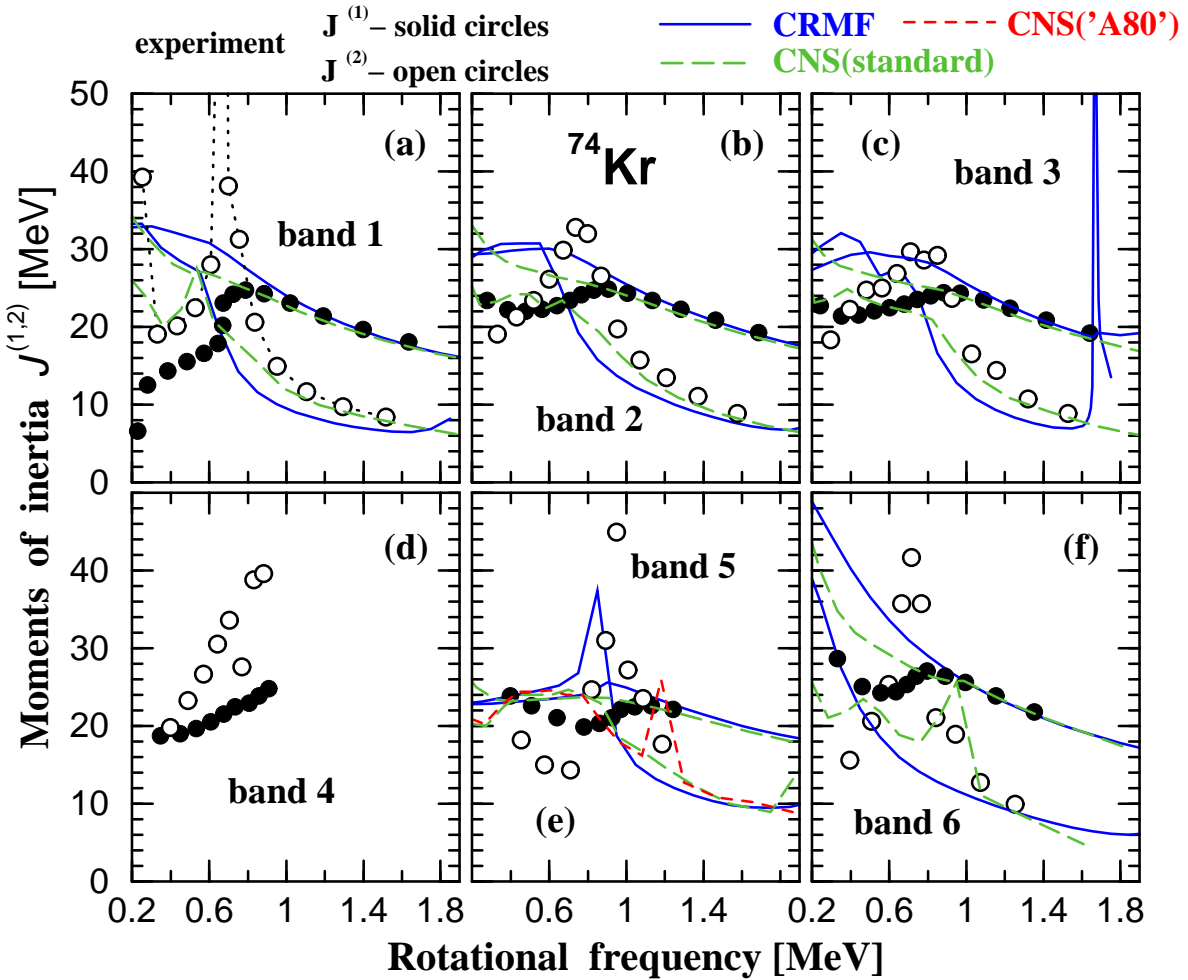


FIG. 3. Dynamic ($J^{(2)}$) and kinematic ($J^{(1)}$) moments of inertia of observed bands in ^{74}Kr and corresponding calculated configurations. The results of the CNS and CRMF calculations are shown by different lines: the line being lowest at medium frequency corresponds to $J^{(2)}$, while highest one to $J^{(1)}$. The results of the CNS calculations with the 'A80' set of the Nilsson parameters are shown only when they differ considerably from those obtained with the standard parameters. Experimental data are taken from Refs. [36,40].

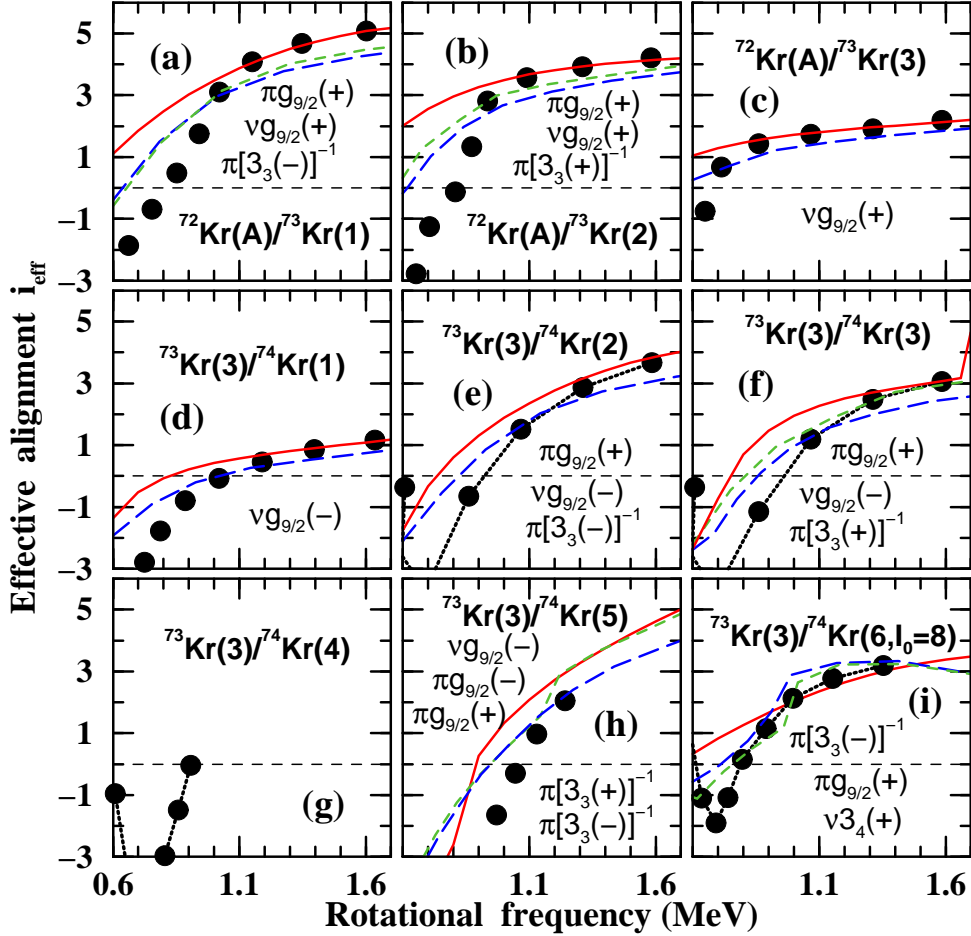


FIG. 4. Effective alignments i_{eff} (in units \hbar) of pairs of bands. The experimental values (solid circles) are compared with the ones calculated from the configurations assigned to the bands. The experimental effective alignment between bands A and B is indicated as “A/B”. The band A in the lighter nucleus is taken as a reference so the effective alignment measures the effect of additional particle(s)/hole(s). In order to guide eye, the solid circles are linked by dotted lines in a few cases. The compared configurations differ by the occupation of the orbitals indicated on the panels. The sign of signature α of the orbital is given in parentheses behind the orbital label. 3_i refers to the i -th low- j $N = 3$ orbital, while superscript ‘ -1 ’ indicates the hole in a given orbital. Solid, long-dashed and short-dashed lines are used for the effective alignments obtained in the CRMF, CNS (standard Nilsson parameters) and CNS ('A80' Nilsson parameters) calculations, respectively. The latter results are shown only if they differ from the ones with the standard Nilsson parameters by more than $0.25\hbar$.

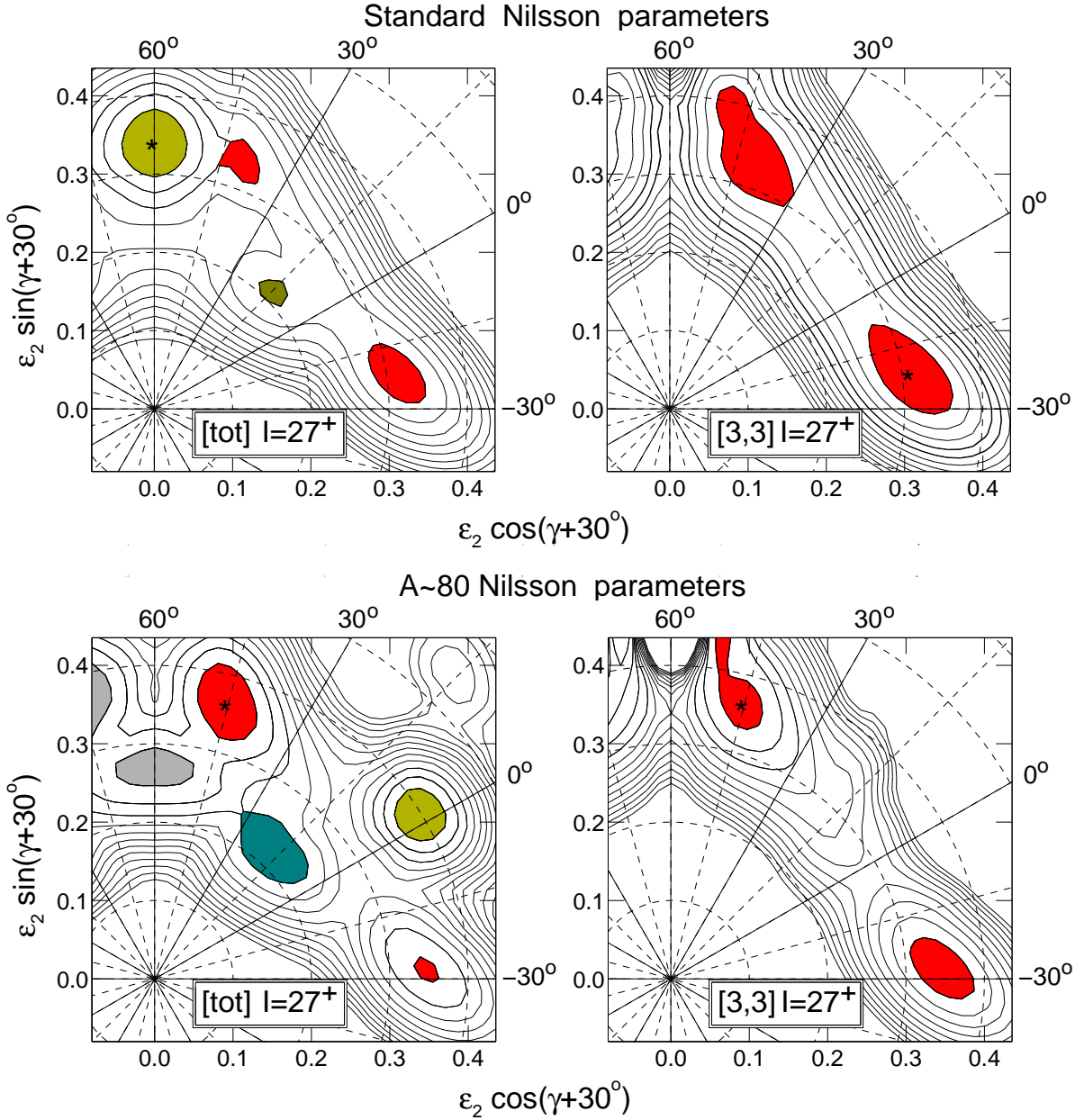


FIG. 5. Potential energy surfaces in ^{70}Br for spin $I = 27^+$. In the left panels only parity ($\pi = +$) and signature ($\alpha = 1$) are fixed. In the right panels only the [3,3] configuration is shown. The contour line separation is 0.25 MeV. The last equipotential line corresponds to 3.0 MeV excitation with respect to the global minimum. The local minima, the excitation of which with respect of the global minimum does not exceed 1.0 MeV, are shaded. The results with the standard and 'A80' Nilsson parameters are presented in top and bottom panels, respectively.

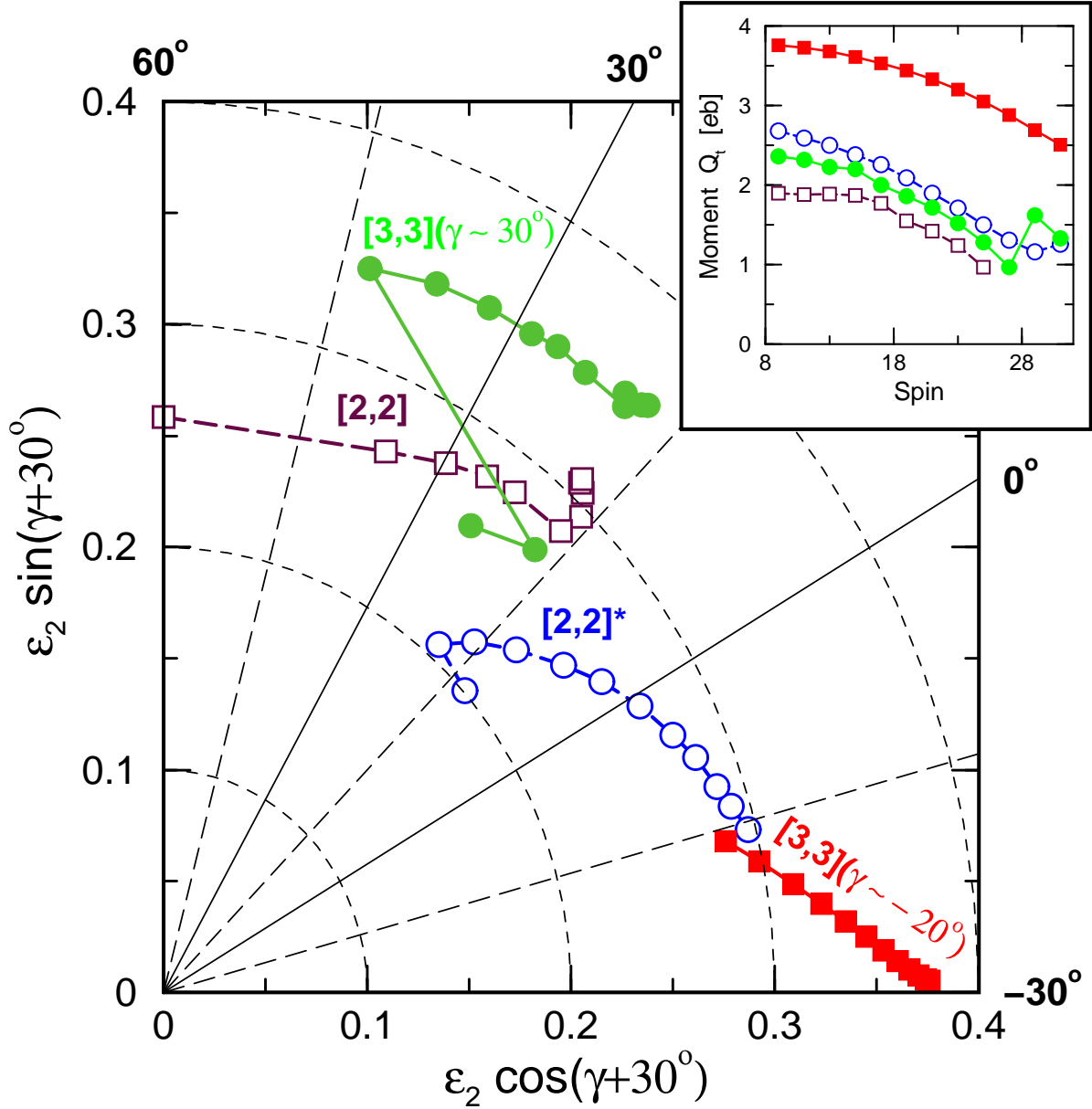


FIG. 6. The calculated shape trajectories of the $[2,2]$ and $[3,3]$ configurations in ^{70}Br . The corresponding transition quadrupole moments Q_t are shown in the insert. The shape trajectories are shown for $9\hbar \leq I \leq 31\hbar$ in steps of $2\hbar$. The $[2,2]$ configuration terminates at $I = 27\hbar$. The initial point on right side of each trajectory corresponds to the lowest spin.

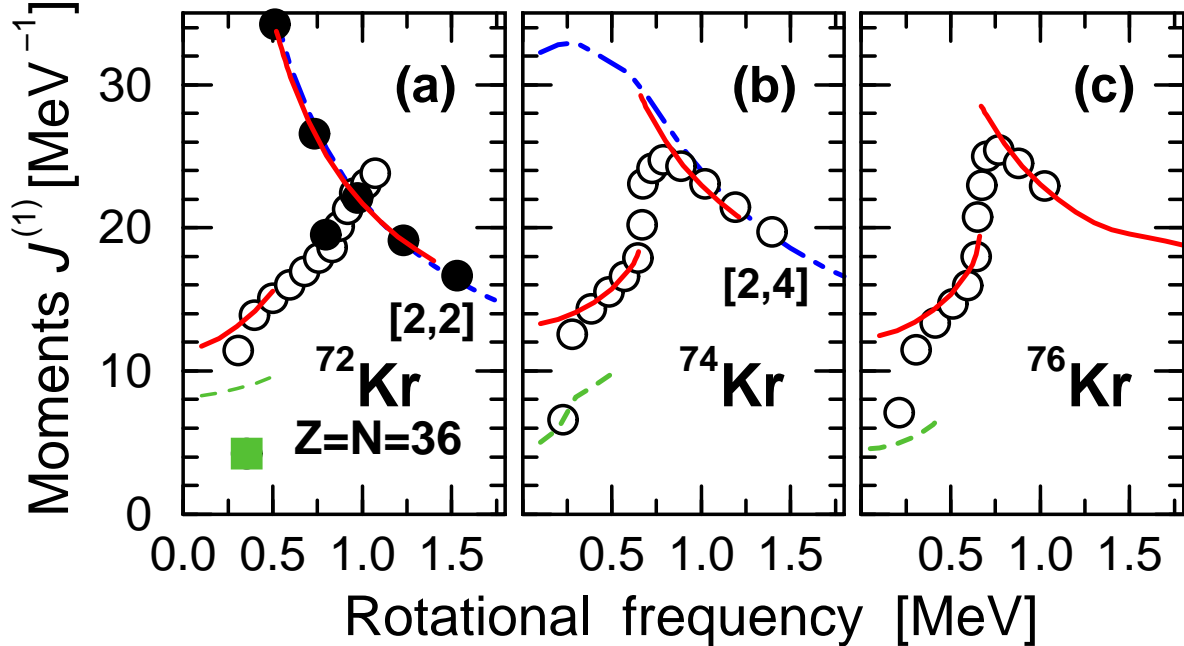


FIG. 7. Experimental (symbols) and calculated (lines) kinematic moments of inertia in $^{72,74,76}\text{Kr}$. The results of the CRHB+LN calculations for the yrast configurations in the near-prolate and the near-oblate (only at low ω) minima are shown. In addition, the results of the CRMF calculations for the lowest configuration in the prolate minimum are displayed. Bands A, B and C in ^{72}Kr are shown by solid circles, open circles and solid squares, respectively. The $J^{(1)}$ value corresponding to the linking transition between bands A and B with energy 1588 keV is included in the curve of band A in order to visualise the backbending. The experimental data are taken from Refs. [49] (^{72}Kr), [40] (^{74}Kr) and [37] (^{76}Kr). Solid and long-dashed lines are used for the CRHB+LN results in near-prolate and near-oblate minima, respectively. The CRMF results for unpaired analogs of the S-bands are shown by dot-dashed lines.

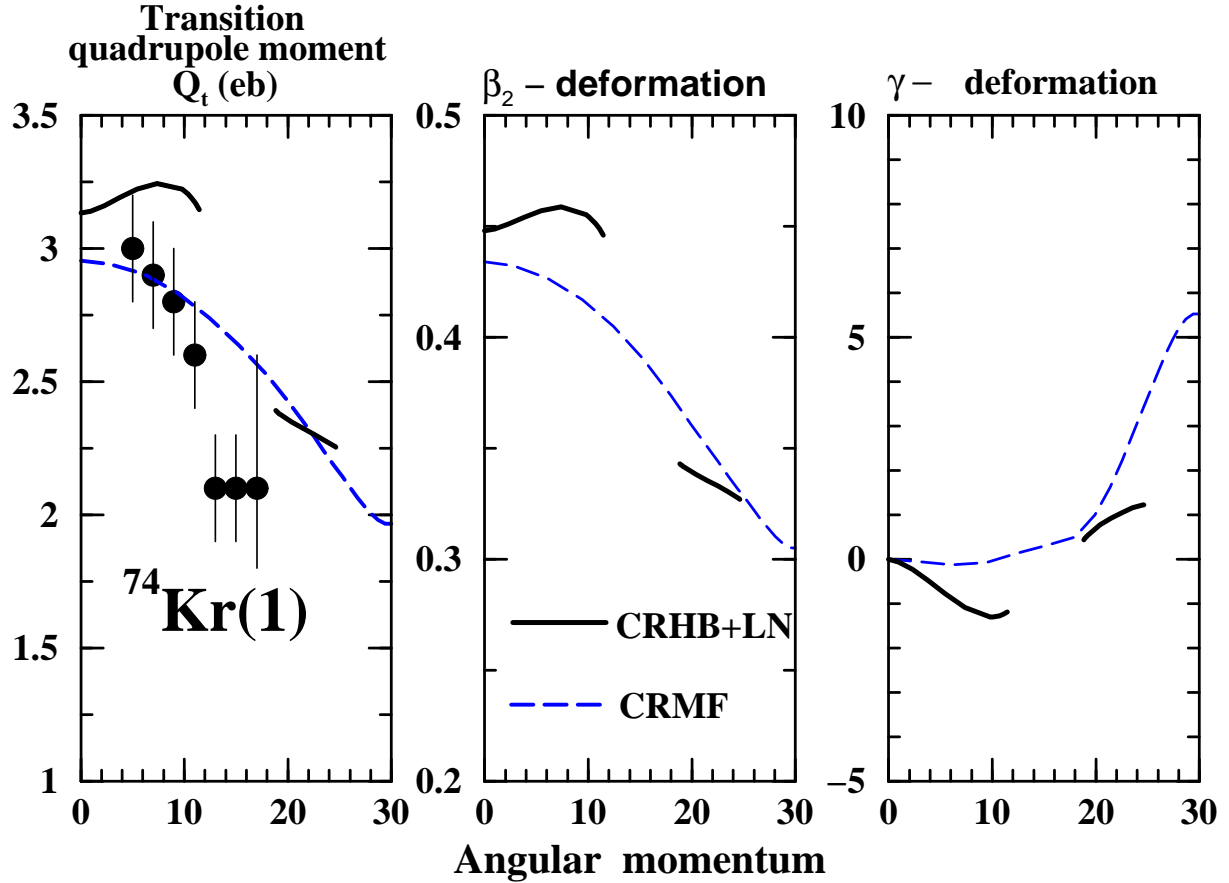


FIG. 8. Deformation properties of the ground state band in ^{74}Kr . Experimental data are taken from Ref. [39]. The results of the CRHB+LN and CRMF (for the [2,4] configuration) calculations are shown by solid and dashed lines, respectively.

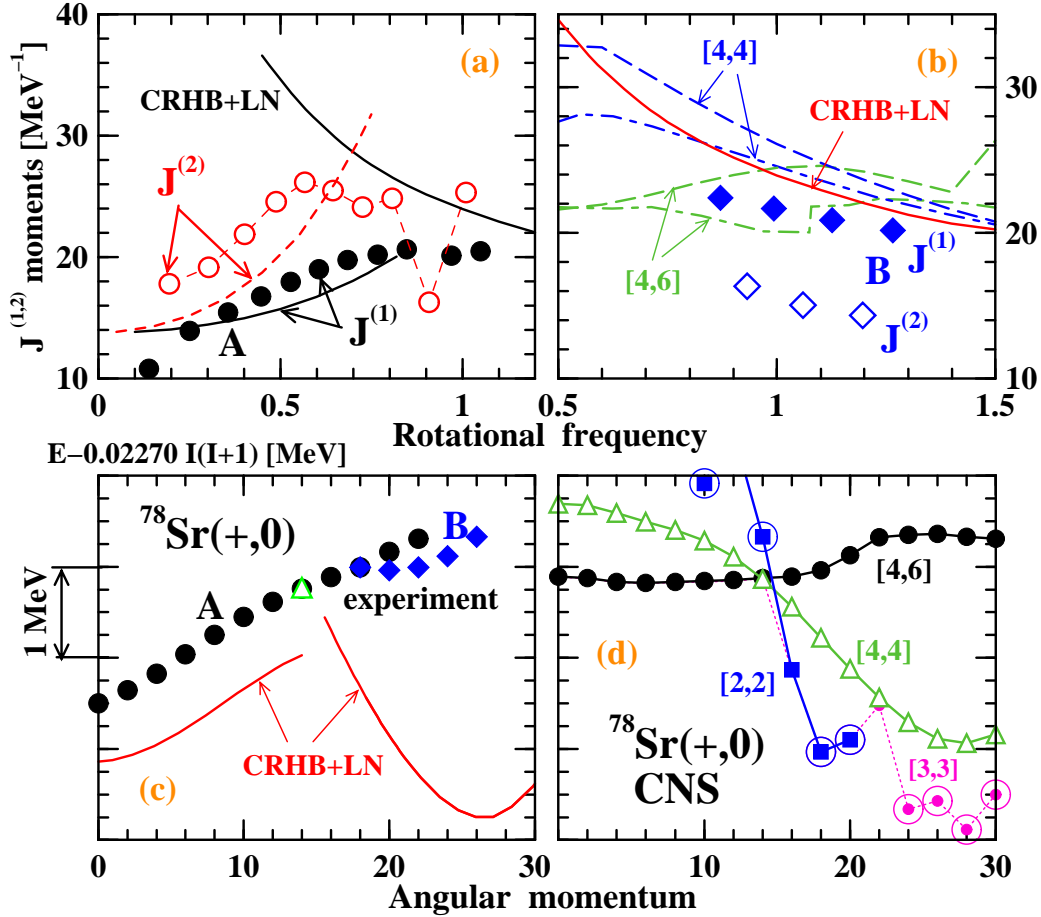


FIG. 9. Panel (a): Kinematic (solid symbols) and dynamic (open linked symbols) moments of inertia of branch A in ^{78}Sr compared with the CRHB+LN results. Calculated $J^{(1)}$ and $J^{(2)}$ (only up to back-bending) values are shown by solid and dashed lines, respectively. Panel (b): the same as in panel (a) but for the branch B. The CRHB+LN, CRMF and CNS results for $J^{(1)}$ are shown by solid, long-dashed and dot-dashed lines, respectively. (c) Excitation energies of the ($\pi = +, \alpha = 0$) structures (unlinked symbols) compared with the results of the CRHB+LN calculations (solid lines). They are given with respect of the rigid rotor reference. (d) The CNS results for the yrast and near-yrast collective and non-collective structures with ($\pi = +, \alpha = 0$) shown in the same way as in panel (c). The yrast line is indicated by a dotted line.

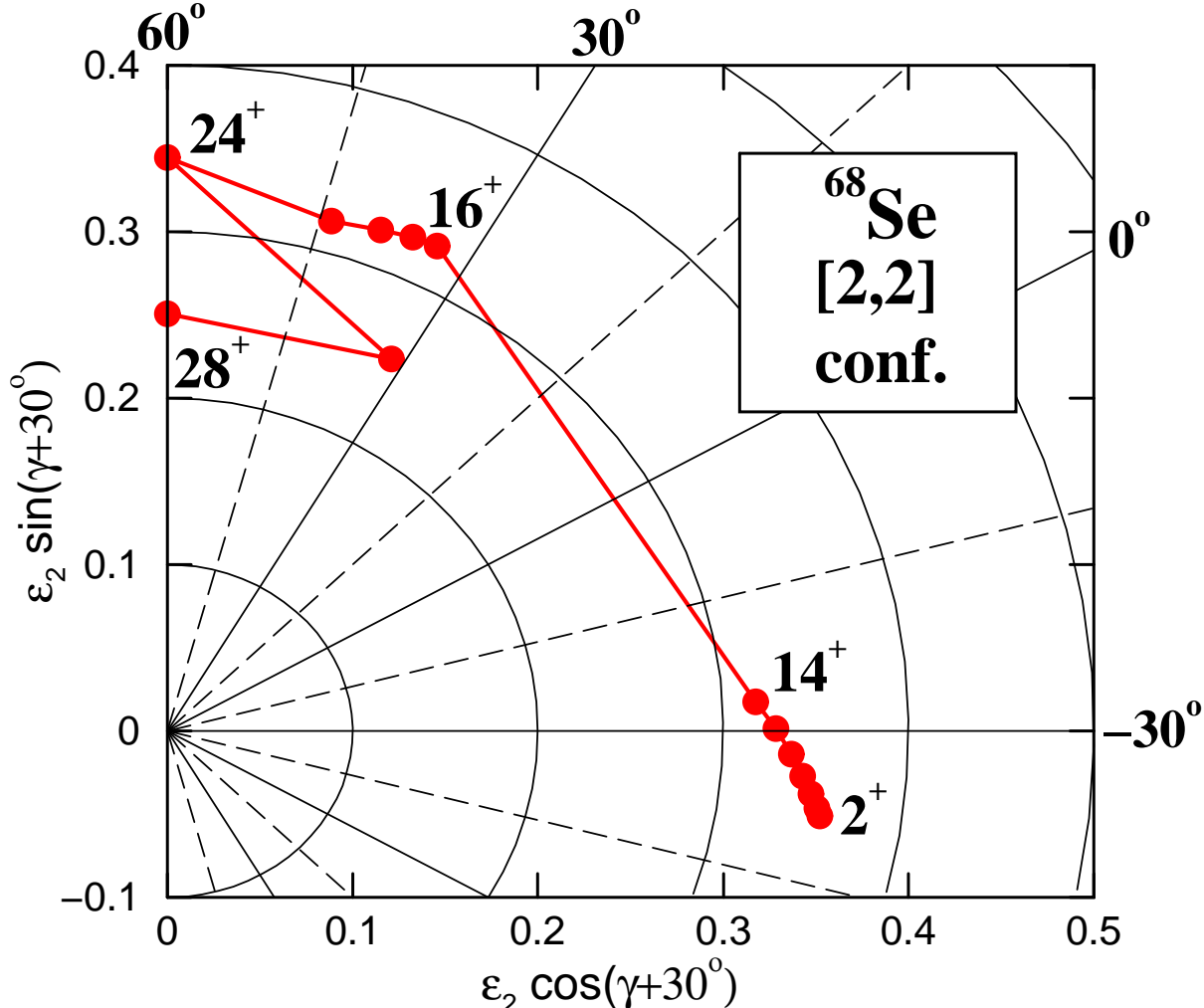


FIG. 10. The calculated (CNS) shape trajectory of the [2,2] configuration in ^{68}Se . The angular momentum changes in steps of $2\hbar$ in the indicated spin range.

FIG. 11. Excitation energies of the configurations forming the yrast lines of 4 combinations of parity and signature in ^{64}Ge relative to a rigid rotor reference $E_{RLD} = 0.03157I(I + 1)$ MeV. Calculated terminating (aligned) states are encircled. The shorthand notation $\langle p_1 p_2, n_1 n_2 \rangle$ indicates the number $p_1(n_1)$ of occupied $g_{9/2}$ proton (neutron) orbitals and the number $p_2(n_2)$ of occupied $h_{11/2}$ proton (neutron) orbitals. $p_2(n_2)$ are omitted when the latter orbitals are not occupied. The wide line indicates the total yrast line. The same type of symbols is used for signature partner orbitals. Solid (open) symbols are used for $\alpha = 0(1)$ configurations.

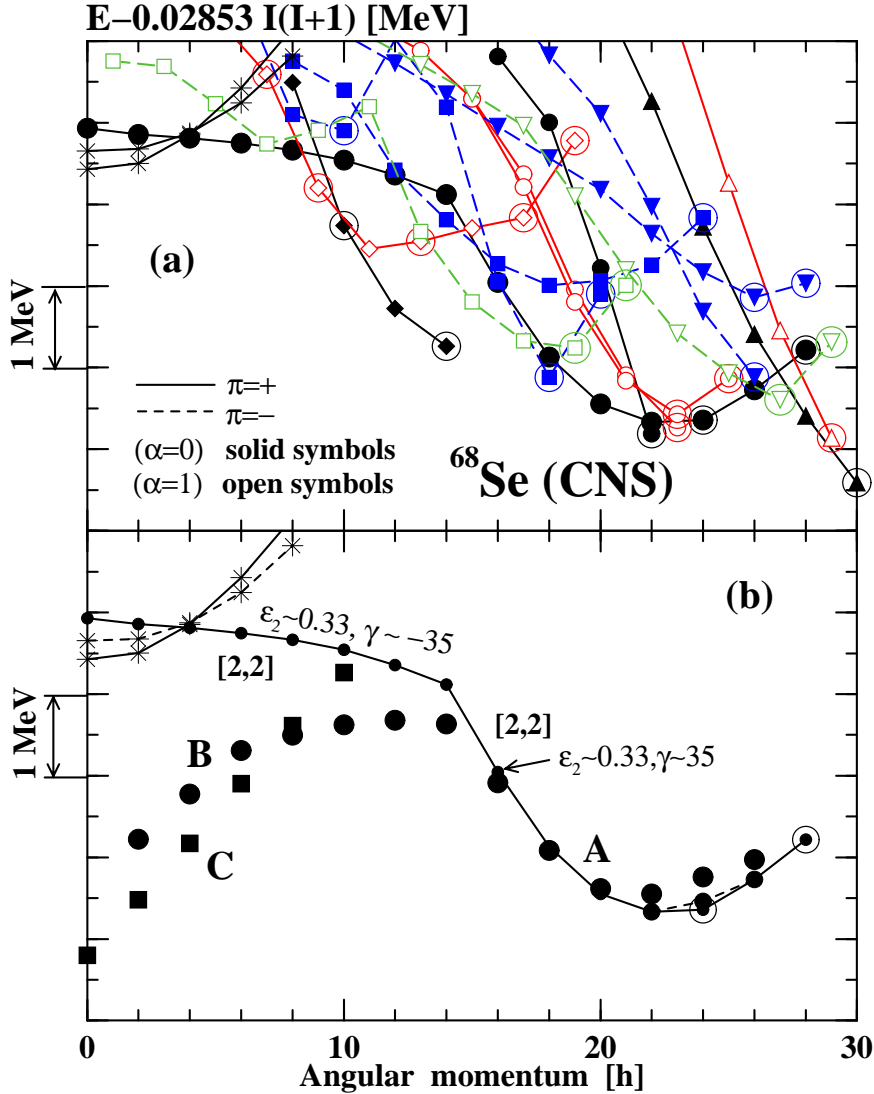


FIG. 12. (a) Excitation energies of the configurations forming the yrast line relative to a rigid rotor reference $E_{RLD} = 0.02853I(I + 1)$ MeV. The calculated terminating (aligned) states are encircled. Only the yrast ($\pi = +, \alpha = 0$) configurations are shown for $I \leq 10\hbar$. Different symbols are used for different types of configurations: stars - [0,0], diamonds - [1,1], squares - [2,1], circles - [2,2], triangles down - [3,2], triangles up - [21,2]. (b) The same as panel (a) but for experimental bands shown by unlinked symbols and assigned configurations shown by lines with symbols. Squares and circles are used for rotational sequences C and A/B, respectively. The data are taken from Ref. [49].

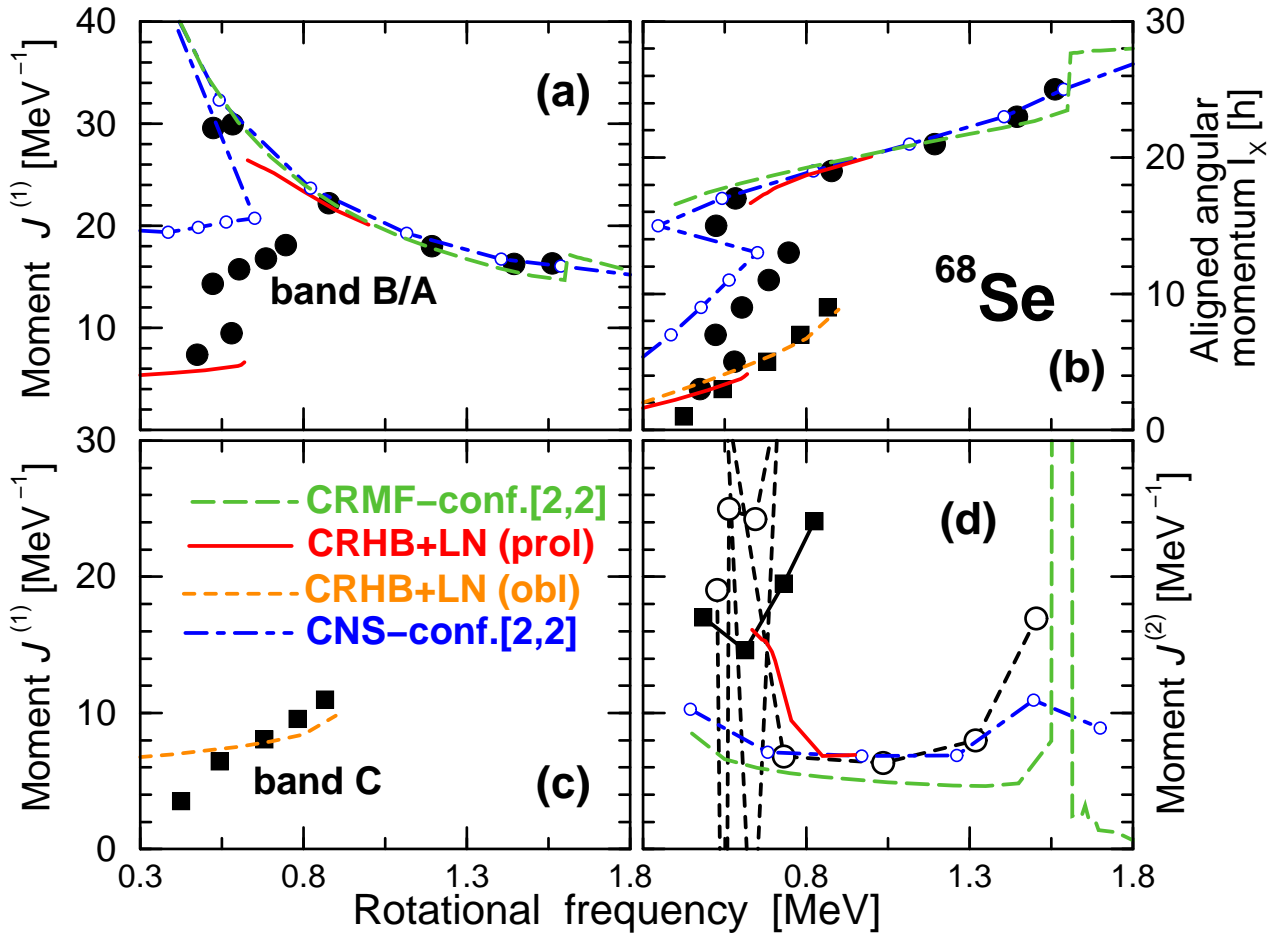


FIG. 13. Kinematic moments of inertia (panels a,c), aligned angular momentum (panel b), and dynamic moments of inertia (panel d) in ^{68}Se as functions of rotational frequency. The data from Ref. [49] are compared with the results of CRHB+LN (in prolate and oblate minima), CRMF (only in the minimum with positive γ) and CNS calculations. The CRHB+LN results in the oblate minimum (panel (c)) are shown only up to the frequency of the band crossing ($\omega = 0.91$ MeV).

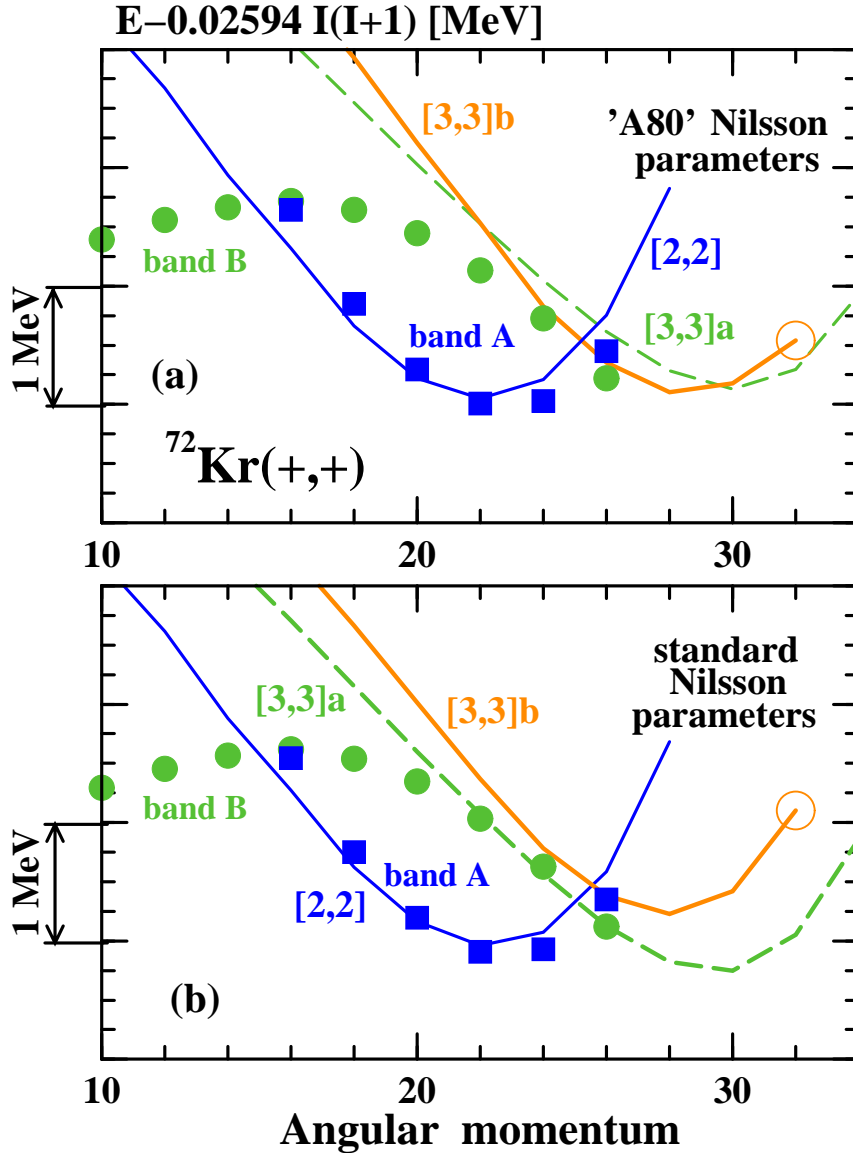


FIG. 14. Calculated yrast and near-yrast collective configurations with $\pi = +, \alpha = 0$ versus observed bands A and B in ^{72}Kr . The excitation energies are given relative to a rigid rotor reference $E_{RLD} = 0.02594I(I + 1)$ MeV. The CNS calculations were performed with the 'A80' (panel (a)) and standard (panel (b)) Nilsson parameters. The experimental data are taken from Ref. [49].

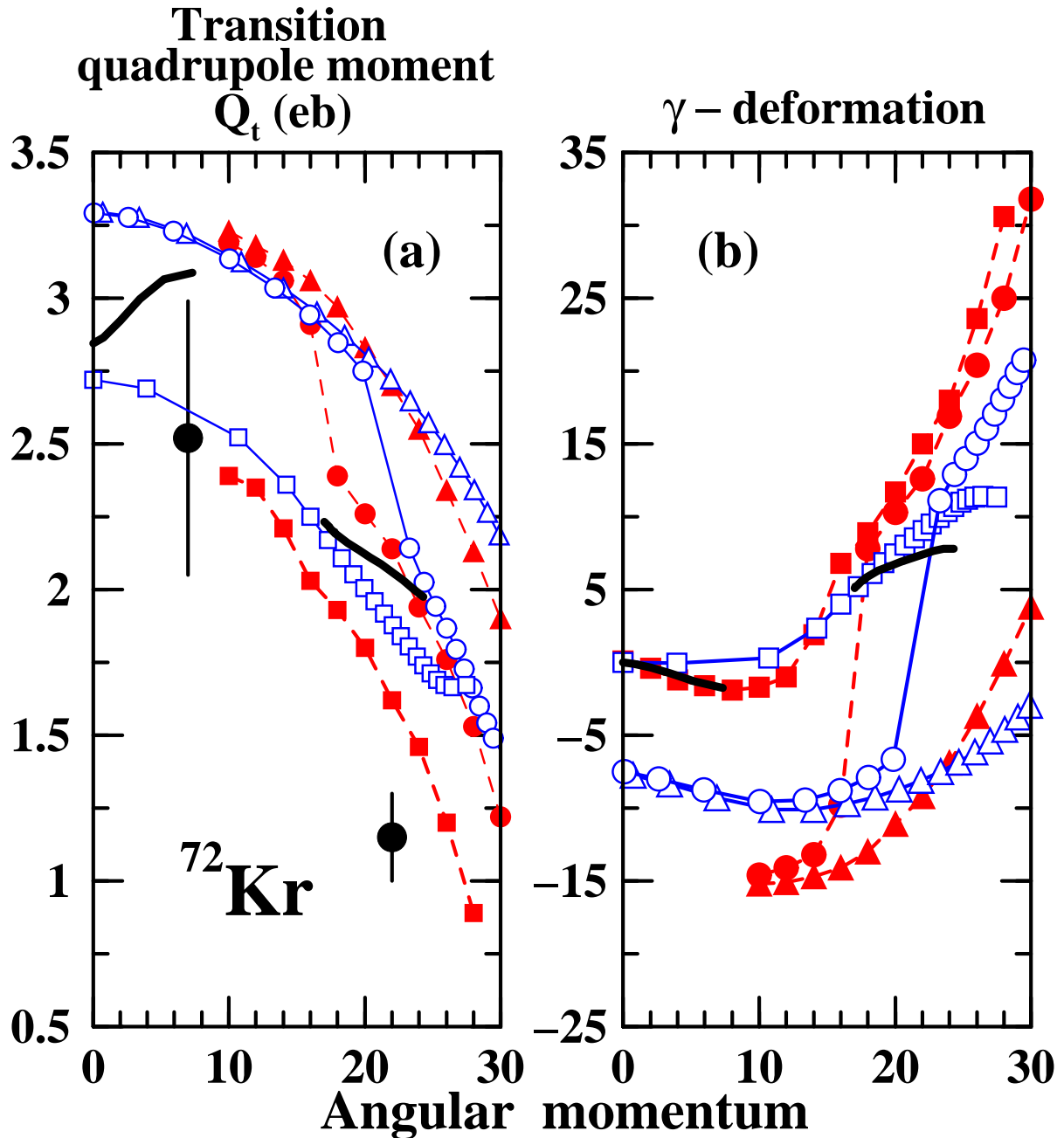


FIG. 15. Transition quadrupole moments Q_t (panel (a)) and γ -deformations (panel (b)) of the calculated configurations in ^{72}Kr . The results of the CNS and CRMF calculations are shown by the solid and open symbols, respectively. The results of the CRHB+LN calculations for the ground state band in the prolate minimum are shown by thick solid lines. Squares, triangles and circles are used for the [2,2], [3,3]a and [3,3]b configurations, respectively. The experimental data are taken from Refs. [55,49].

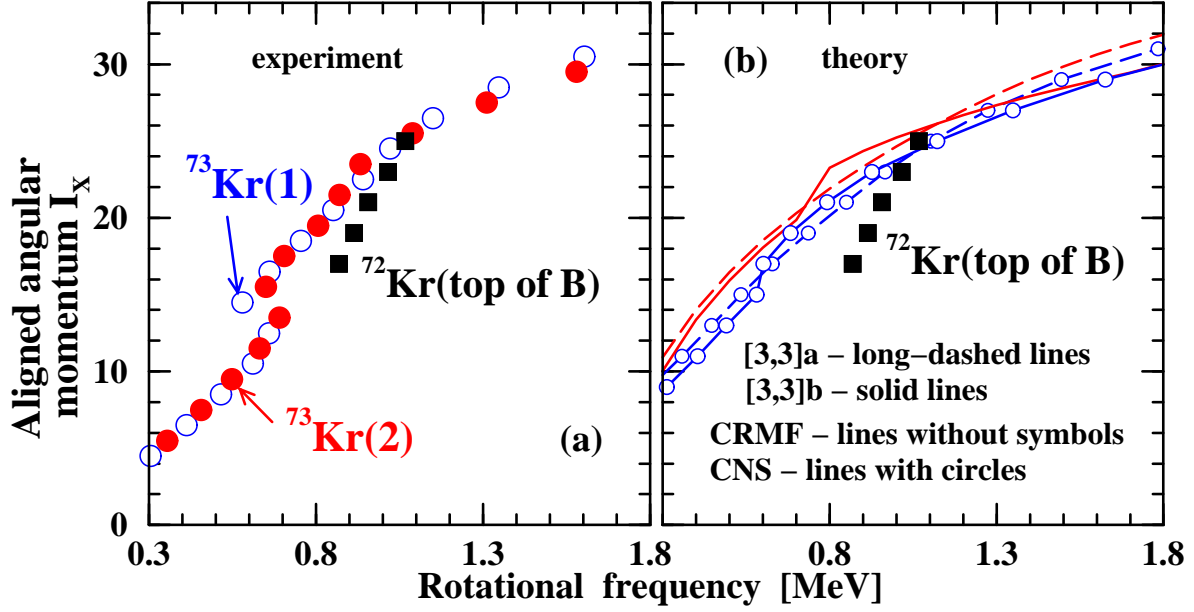


FIG. 16. Angular momentum I_x aligned with the rotation axis as a function of rotational frequency. Panel (a) compares bands 1 and 2 in ^{73}Kr with the top branch of band B in ^{72}Kr . Panel (b) compares the top branch of band B with the results of the CNS (standard Nilsson parameters) and CRMF calculations.

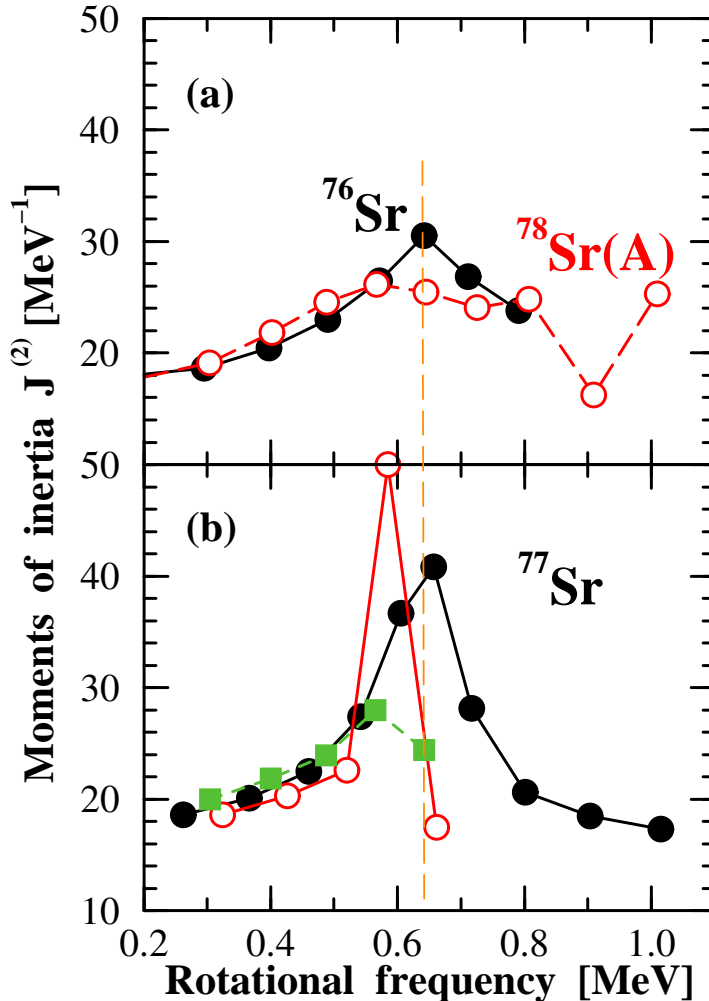


FIG. 17. Dynamic moments of inertia of the ground state bands in $^{76,78}\text{Sr}$ (panel (a)) and of the one-quasiparticle bands in ^{77}Sr (panel (b)). The data are taken from Refs. [43,40,46]. In the bottom panel, solid and open symbols are used for the $\alpha = 1/2$ and $\alpha = -1/2$ bands, respectively. Positive and negative parity bands are denoted by the circles and squares, respectively. The vertical long-dashed line indicates the crossing frequency in the ground state band of ^{76}Sr .

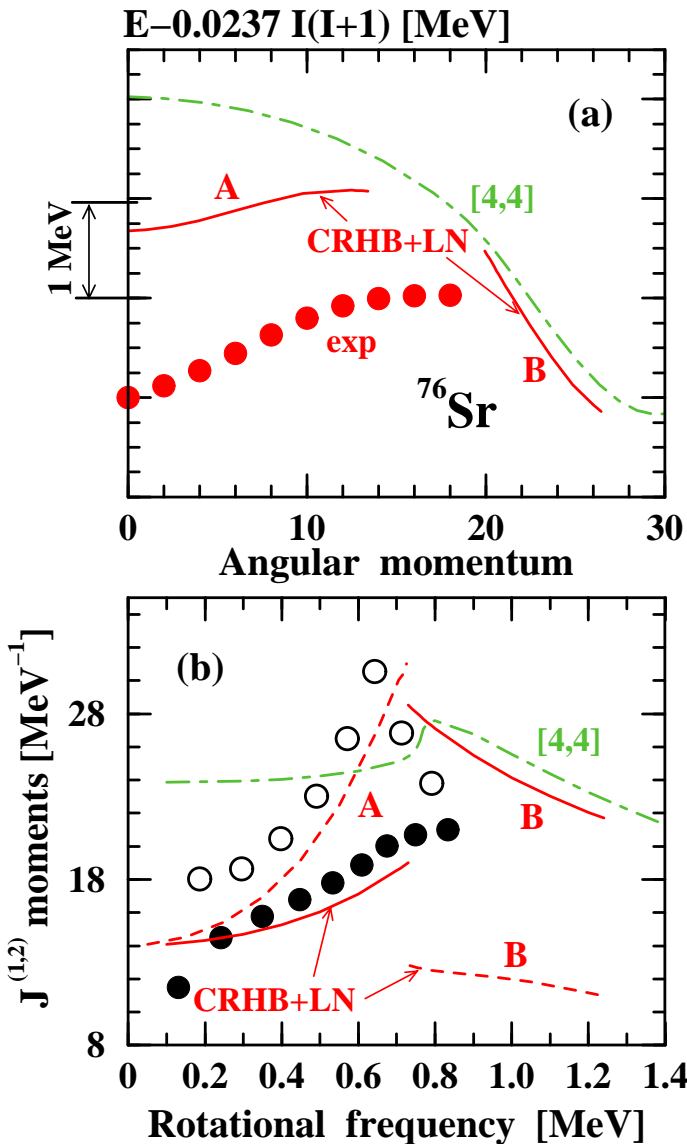


FIG. 18. Panel (a): Excitation energies of the ground state band in ^{76}Sr (circles) compared with the CRHB+LN (solid lines) and the CRMF (dot-dashed line) calculations. The energies are given with respect to the rigid rotor reference $E_{RLD} = 0.0237 I(I + 1)$ MeV. Panel (b): Kinematic (solid symbols) and dynamic (open symbols) moments of inertia of the ground state band in ^{76}Sr compared with the CRHB+LN and CRMF results. Solid and dashed lines are used for kinematic and dynamic moments of inertia obtained in the CRHB+LN calculations. The dot-dashed line shows the kinematic moment of inertia obtained in the CRMF calculations. The experimental data are taken from Ref. [43].

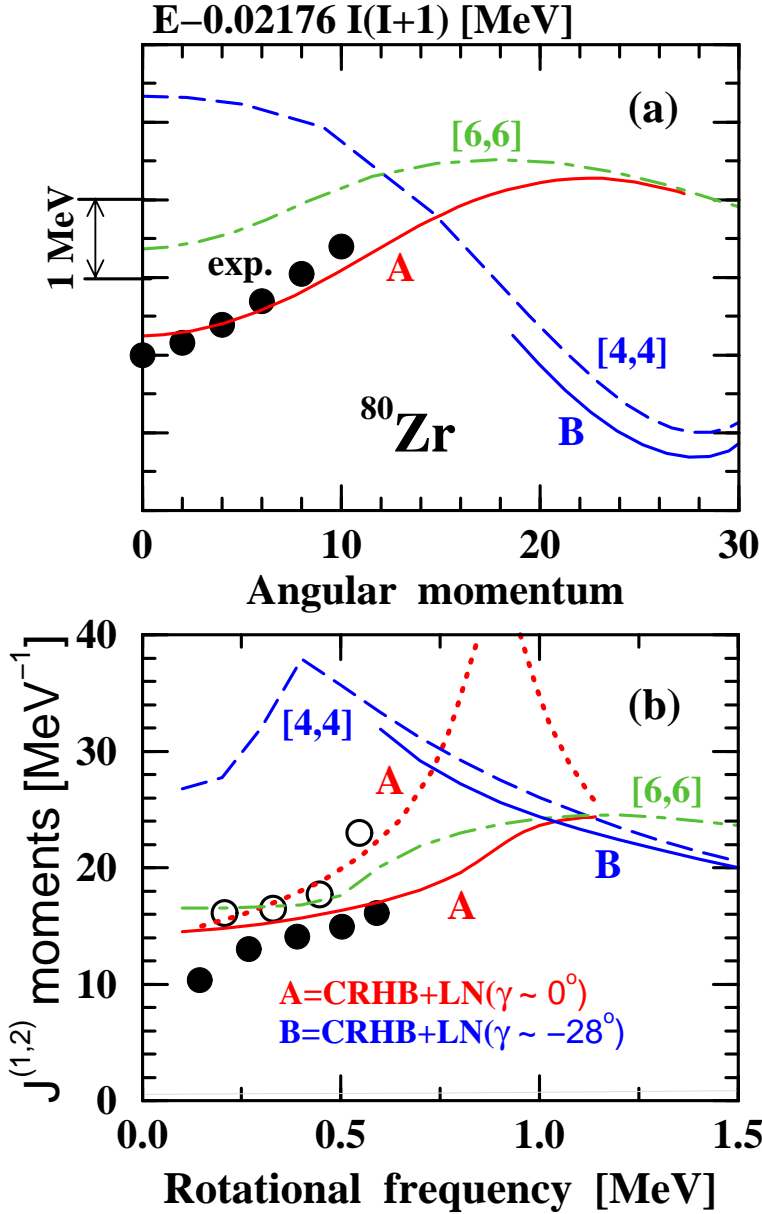


FIG. 19. Panel (a): Excitation energies of the ground state band in ^{80}Zr (unlinked symbols) compared with the results of the CRHB+LN (solid lines) and the CRMF (dashed line) calculations. The energies are given with respect of the rigid rotor reference $E_{RLD} = 0.02176I(I+1)$ MeV. Panel (b): Kinematic (solid symbols) and dynamic (open linked symbols) moments of inertia of ground state band in ^{80}Zr compared with the CRHB+LN and CRMF results. The experimental data are taken from Ref. [43]. The dotted line is used for the dynamic moment of inertia of configuration A, while other lines are used for the kinematic moments of inertia.